Check for updates

RESEARCH ARTICLE

REVISED Elastically induced phase-shift and birefringence in optical fibers

[version 2; peer review: 3 approved]

Elisabeth Steininger[1,2], Thomas Mieling[1], Piotr T. Chruściel[1]

[1]Faculty of Physics and Research Network TURIS, University of Vienna, Vienna, Vienna, 1090, Austria
[2]Faculty of Physics, Vienna Doctoral School in Physics,, University of Vienna, Vienna, Vienna, 1090, Austria

v2 **First published:** 07 Apr 2025, **5**:99
https://doi.org/10.12688/openreseurope.19414.1
Latest published: 13 Aug 2025, **5**:99
https://doi.org/10.12688/openreseurope.19414.2

Abstract

Background

Light propagation in optical fibers is known to be sensitive to ambient conditions such as changes in temperature and pressure. Building on a model for elastic deformations of optical fiber spools derived in previous work, the induced effects on phase and birefringence are investigated.

Methods

We use a perturbative scheme to solve, to first order, the Maxwell equations in deformed fibers using a multiple-scales approximation scheme. Specifically, we consider differences in wave-guiding properties of straight fibers subject to different external temperatures, pressures, and gravitational fields.

Results

We obtain propagation equations for the Jones vector along optical fibers. This results in phase shifts and birefringence effects, for which we derive explicit expressions.

Conclusions

The phase shift can be expressed in terms of the average radial pressure, longitudinal tension, and change in temperature, while birefringence depends on the quadrupole of the external pressure distribution and the stresses on the axis of the fiber. Our result provides stringent constraints on the environmental control needed

Open Peer Review

Approval Status ✓ ✓ ✓

	1	2	3
version 2 (revision) 13 Aug 2025	✓ view		✓ view
version 1 07 Apr 2025	? view	✓ view	? view

1. **M. S. Mani Rajan**, Anna University, Ramanathapuram, India
2. **Xiaohui Li**, Shaanxi Normal University, Xi'an, China
3. **Matthew Maitra**, ETH Zurich, Zürich, Switzerland

Any reports and responses or comments on the article can be found at the end of the article.

for sensitive fiber interferometry.

Keywords
linear elasticity, GRAVITES, waveguides, optical fibers, Maxwell, photoelasticity, single mode fibers, multiple-scales analysis



This article is included in the Horizon Europe gateway.



This article is included in the European Research Council (ERC) gateway.

Corresponding author: Elisabeth Steininger (elisabeth.steininger@univie.ac.at)

Author roles: Steininger E: Conceptualization, Formal Analysis, Investigation, Methodology, Software, Visualization, Writing – Original Draft Preparation, Writing – Review & Editing; **Mieling T**: Conceptualization, Methodology, Validation, Writing – Original Draft Preparation, Writing – Review & Editing; **Chruściel PT**: Conceptualization, Funding Acquisition, Project Administration, Supervision, Writing – Original Draft Preparation, Writing – Review & Editing

Competing interests: No competing interests were disclosed.

Grant information: This project has received funding from the European Research Council (ERC) under the European Union's Horizon Europe research and innovation programme (Grant agreement No. 101071779). E.S. was supported in part by the Austrian Science Fund (FWF), Project P34274. Views and opinions expressed are however those of the authors only and do not necessarily reflect those of the European Union or the European Research Council Executive Agency. Neither the European Union nor the granting authority can be held responsible for them.
The funders had no role in study design, data collection and analysis, decision to publish, or preparation of the manuscript.

Copyright: © 2025 Steininger E *et al*. This is an open access article distributed under the terms of the Creative Commons Attribution License, which permits unrestricted use, distribution, and reproduction in any medium, provided the original work is properly cited.

How to cite this article: Steininger E, Mieling T and Chruściel PT. **Elastically induced phase-shift and birefringence in optical fibers [version 2; peer review: 3 approved]** Open Research Europe 2025, **5**:99 https://doi.org/10.12688/openreseurope.19414.2

First published: 07 Apr 2025, **5**:99 https://doi.org/10.12688/openreseurope.19414.1

REVISED **Amendments from Version 1**

Improved write-up taking into account the feedback provided by the reviewers, for which we are grateful.

In particular we clarified some of the underlying assumptions of this project, such as the restriction to linear and isotropic media and how this relates to the broader research context.

We elaborated on some of the implications for the GRAVITES experiment in Section 4.

Section 3 was enhanced by making the coordinate transformations more explicit.

Small corrections throughout.

Any further responses from the reviewers can be found at the end of the article

1 Introduction

Long-baseline interferometry can be carried out with formidable precision in tabletop experiments using optical fibers, enabling the measurement of small effects on the propagation of single-photons, such as the Sagnac effect[1–3]. Yet another example is provided by an experiment that is being built to measure phase shifts arising from vertical displacements of one arm of the interferometer in the gravitational field of the Earth[4,5]. Compared to experiments involving light propagation in vacuum, one faces the challenge of minimizing, controlling, and compensating for noise arising inside the fiber, or arising from the response of fibers to changes, drifts, and fluctuations of ambient conditions[6]. In particular, for experiments that modulate their signal by moving one or both interferometer arms as, e.g., in Refs. [4, 5], the resulting tiny local variations in pressure, temperature, or local gravity, lead to elastic deformations of the fibers that influence light propagation. It is necessary to model these effects accurately in order to extract, from the data, the signal which one aims to measure. Indeed, one needs to calculate the phase shifts associated with such changes, to determine the level of control of the environmental variables needed to be able to draw conclusions from the experimental data. The aim of this work is to carry this out. While we focus on the effects relevant for the planned GRAVITES experiment[4], our results apply to any extreme-precision optical fiber experiments, where small variations of pressure or temperature are unavoidable, even in vacuum.

A simplified schematic diagram of this last experiment is shown in Figure 1.1. The interferometer aims to measure phase shifts induced by Earth's gravity on entangled multi-photon states propagating in optical fibers. To modulate this effect, one interferometer arm is gradually lifted by 1 m relative to a stationary reference arm. If the fiber length is held constant in the process, the gravitational redshift implies a difference in phase for the two interferometer arms, which results in a height-dependent change in detection statistics of individual photons at the two output ports of the final beam-splitter. Now, the gravitational field in the laboratory changes with height. Moreover, the pressures and temperatures at the two interferometer arms are, in general, not equal. The differences in gravitational acceleration, ambient pressure, and ambient temperature, will be denoted by $\delta\mathrm{g}$, δ, and δT.

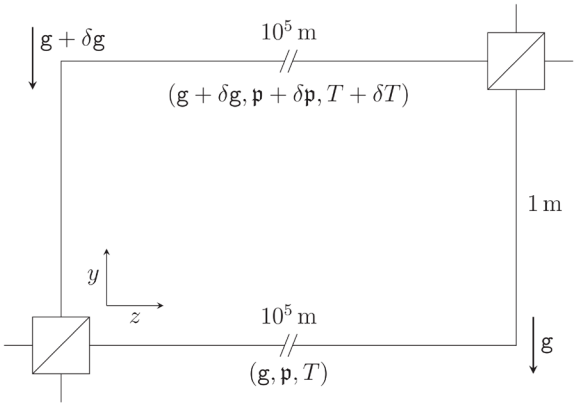

Figure 1.1. Schematic representation of the GRAVITES experiment[4]. Light propagates through optical fibers in two vertically separated arms of an interferometer and traverses spools with a total fiber length of the order of 100km, accumulating different phases due to the gravitational redshift. We consider a simplified setup as in previous work[7], where the spools are unwound and treated as straight fiber sections. We allow for a difference in gravitational acceleration $\delta\mathrm{g}$, ambient pressure δ and ambient temperature δT at the spool locations, leading to elastic effects on the photon propagation. This figure has been reproduced with permission[7].

These differences in local parameters affect the wave-guiding properties of the optical fibers both by the photoelastic effect and by changes of length and cross-sectional geometry of the fiber. Here, we determine these effects for linear single-mode fibers, ignoring effects that are not mediated by elasticity such as the thermo-optic effect[8,9].

As such, the elastic response of (straight) optical fibers to variations in gravity, pressure, and temperature, was modeled from first principles in a previous work[7]. We build upon these results by solving Maxwell's equations in so-deformed fibers to determine the effect of variations of ambient parameters on light propagation in single-mode fibers. This is done using the perturbative scheme developed in Refs. 10–12.

This paper is organized as follows. In Section 2 we review the formulation of Maxwell's equations in linear dielectrics in terms of gauge-fixed wave equations for the electromagnetic potential. These equations can be solved explicitly for the case of undeformed and unstrained step-index fibers, yielding the standard mode solutions. Following the approach of Refs. 10,11 and restricting to single-mode fibers, we extend the calculations there to include generic perturbation terms, and derive the general solution to first order in perturbation theory. The final formula contains both polarization-independent phases and contributions from birefringence. This result is then used in the following sections to describe the phase shift and birefringence induced in the fiber by elastic deformations of any origin.

In Section 3 we review the elastic deformations of optical fibers derived in Ref. 7, and derive the induced correction terms in the electromagnetic field equations describing light propagation in such fibers. These corrections arise directly from the geometric fiber deformation (that alters the shape of the core-cladding interface), and indirectly through the induced anisotropy (arising from the strain due to photoelasticity). To first order in perturbation theory these effects add and can thus be computed separately: In Section 3.1 we describe the purely geometric deformation effects, and in Section 3.2 we discuss the photoelastic effects. The resulting expressions for the phase shifts and birefringence contain integrals that need to be evaluated numerically.

Figure 1.2 and Figure 1.3 summarize the results of our analysis and can be viewed as the main result of this paper.

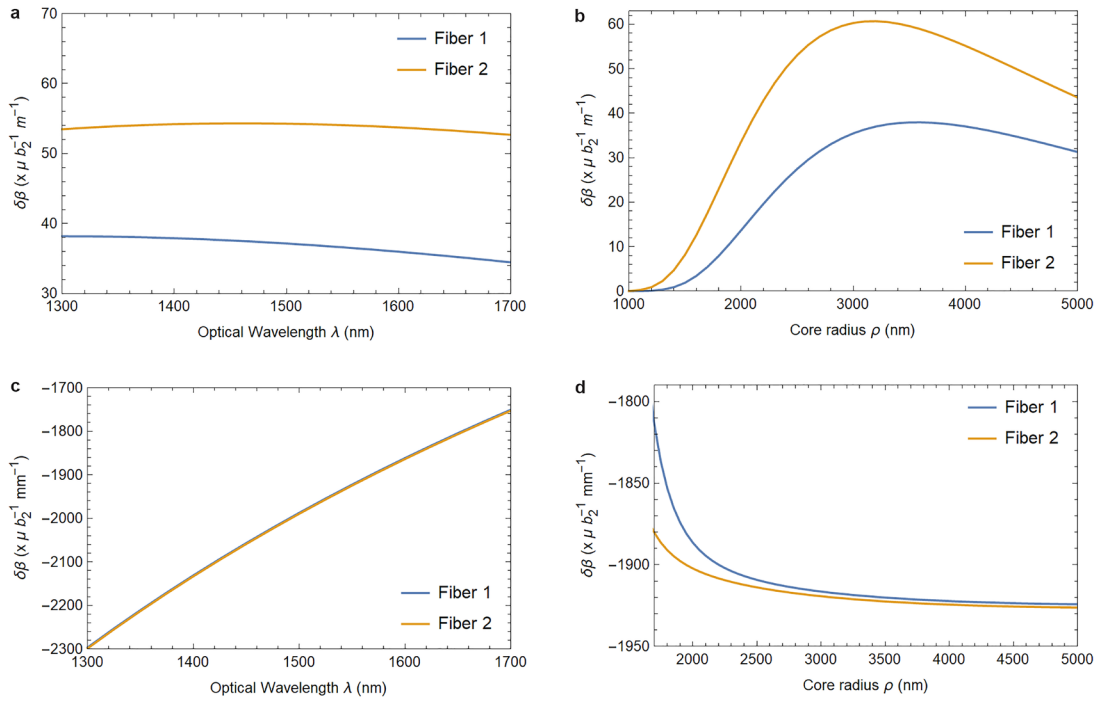

Figure 1.2. Varying the wavelength (left column) or the fiber core radius (right column) changes the birefringence induced by the elastically deformed core-cladding interface (1.2a and 1.2b) and the birefringence caused by the photoelastic material response (1.2c and 1.2d). Fiber 1 describes a fiber with parameters as listed in Table 3.1–Table 3.2, and Fiber 2 has refractive indices $n_1 = 1.4715$ and $n_2 = 1.4648$ instead, with the fibers identical otherwise. The parameter b_2 quantifies the strain in the waveguide as defined in (3.11). In Figure 1.2c, and in the physically relevant region of Figure 1.2d, both fiber's responses are identical for all practical purposes.

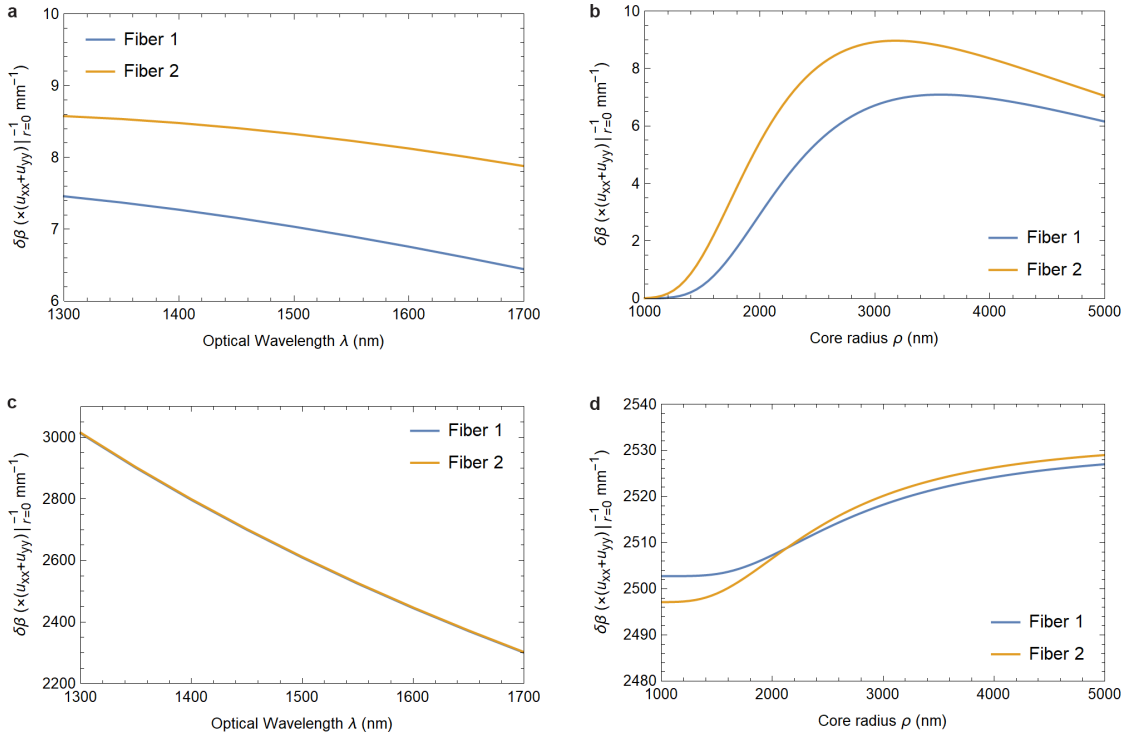

Figure 1.3. Figure 1.3a and Figure 1.3b show the dependence of the phase shift on the elastic deformation of the core-cladding interface as functions of the optical wavelength and the fiber's core radius. Figure 1.3c and Figure 1.3d, on the other hand, show the dependence of the photoelastically induced phase shift on these parameters. The material parameters are the same as in Figure 1.2. In Figure 1.3c, and in the physically relevant region of Figure 1.3d, the responses of both fibers are identical for all practical purposes.

In Section 3.3 we provide numerical results with parameters relevant for the GRAVITES experiment.

Our calculations are presented in units in which the vacuum permeability μ_0, the vacuum permittivity ϵ_0, and hence also the speed of light in vacuum c, are set to unity. Note that the final formulæ do not involve these constants. Coordinate indices are denoted by μ, ν, …, and range from 0 to 3, while the frame indices are denoted by a, b, …, and range over the set $\{t, z, \sharp, \flat\}$, compare Equation (2.10) below. Implicit summation over repeated indices is employed throughout.

2 Perturbative fiber optics

Let us start by introducing the formalism used to describe electromagnetic modes in deformed single-mode fibers. To solve Maxwell's equations in such fibers it is useful to formulate the equations in curvilinear coordinates adapted to the deformation of the fiber. For this in Section 2.1 we recall a generally covariant formulation of Maxwell's equations in linear dielectrics. As these equations are generally not solvable explicitly, perturbation techniques are required. In our case, the unperturbed reference problem is that of an undeformed fiber, the modes of which are described in Section 2.2. Based on this, in Section 2.3 we present an approximation scheme that allows to compute perturbations of such modes. This scheme is general in that it applies to arbitrary small deviations from unperturbed field equations, regardless of their origin, as long as the perturbations are invariant under translations along the fiber. The results in this section will be used in Section 3 to determine the effects of internal deformations and of stress-induced anisotropy.

2.1 Maxwell's equations in linear media

Maxwell's equations without sources can be written in generally covariant form as

$$\nabla_{[\mu} F_{\mu\nu]} = 0, \tag{2.1a}$$

$$\nabla_{\mu} G^{\mu\nu} = 0, \tag{2.1b}$$

where $F_{\mu\nu}$ and $G^{\mu\nu}$ are antisymmetric tensors describing the electromagnetic field strength and excitation, where ∇_μ is the covariant derivative associated to the space-time metric tensor $g_{\mu\nu}$, and where square brackets indicate antisymmetrization (cf. e.g. 13). To obtain a closed system it is necessary to formulate a *constitutive law* that relates $G^{\mu\nu}$ and $F_{\mu\nu}$. For linear and non-dispersive media, the standard form of this law takes the form

$$G^{\mu\nu} = \chi^{\mu\nu\rho\sigma} F_{\rho\sigma}, \tag{2.2}$$

with the *constitutive tensor* $\chi^{\mu\nu\rho\sigma}$ exhibiting the symmetries

$$\chi^{\mu\nu\rho\sigma} = +\chi^{\rho\sigma\mu\nu} = -\chi^{\nu\mu\rho\sigma} = -\chi^{\mu\nu\sigma\rho}. \tag{2.3}$$

Here we assume that $\chi\mu\nu\rho\sigma$ does not depend on $F_{\mu\nu}$, which excludes non-linearities and dispersion. This linear model provides an adequate approximation of the problem at hand for low light intensities, in particular for the single-photon experiments of interest here. Nonlinear phenomena such as the Kerr effect in Ref. [14, Section 3.14] or the effects described in Refs. [15, 16], are negligible when describing single-photon propagation, which is the focus of this work. We also note that Equation (2.2) is adequate for monochromatic modes, where the dispersion-free model is sufficient. This can be generalized by Fourier analysis using Equation (2.2) for every Fourier mode separately, with dispersive effects arising from a possible frequency-dependence of $\chi\mu\nu\rho\sigma$.

For isotropic dielectrics with four-velocity u^μ, permittivity ϵ, and permeability μ, it can be shown[17] that the constitutive tensor takes the form

$$\chi^{\mu\nu\rho\sigma}_{\text{isotropic}} = \frac{1}{2\mu}(\gamma^{\mu\rho}\gamma^{\nu\sigma} - \gamma^{\mu\sigma}\gamma^{\nu\rho}), \tag{2.4}$$

where $\gamma^{\mu\nu}$ is *Gordon's optical metric*

$$\gamma^{\mu\nu} = g^{\mu\nu} + (1 - n^2)u^\mu u^\nu, \tag{2.5}$$

in which $n = \sqrt{\epsilon\mu}$ is the refractive index.

Optical fibers are often modeled as linear isotropic dielectrics with $\mu = 1$[18]. However, to describe photoelastic effects in fibers, we will allow more general constitutive tensors $\chi^{\mu\nu\rho\sigma}$ that reduce to $\chi^{\mu\nu\rho\sigma}_{\text{isotropic}}$ with $\mu = 1$ in the absence of deformations and stresses.

The following calculations are carried out in terms of an electromagnetic potential A_μ such that

$$F_{\mu\nu} = \nabla_\mu A_\nu - \nabla_\nu A_\mu. \tag{2.6}$$

In this formulation Equation (2.1a) is identically satisfied, and Equation (2.1b) does not directly provide well-posed evolution equations due to the gauge redundancy $A_\mu \to A_\mu + \partial_\mu \lambda$. Following Refs. 10,11,19 we therefore consider the gauge-fixed Lagrangian

$$\mathcal{L} = -\frac{1}{4}\chi^{\mu\nu\rho\sigma}F_{\mu\nu}F_{\rho\sigma} - \frac{1}{2}\chi^2_{\text{gauge}}, \qquad \text{with} \qquad \chi_{\text{gauge}} = \nabla_\mu(\gamma^{\mu\nu}A_\nu), \tag{2.7}$$

where $\gamma^{\mu\nu}$ is the Gordon metric with $\mu = 1$ and $\epsilon = n^2$ being the permittivity of the undeformed reference configuration, without deformations and stresses. The corresponding Euler–Lagrange equations

$$\nabla_\mu G^{\mu\nu} + \gamma^{\mu\nu}\nabla_\mu \chi_{\text{gauge}} = 0 \tag{2.8}$$

reduce to Equation (2.1b) whenever χ_{gauge} vanishes, and are well-posed irrespective of this gauge condition[10].

In everything that follows the metric is taken to be the Minkowski metric, which we denote by $\eta_{\mu\nu}$, and the four-velocity vector is constant throughout the medium. Hence, in the case of an idealized step-index fiber, where $\chi^{\mu\nu\rho\sigma} = \chi^{\mu\nu\rho\sigma}_{\text{isotropic}}$ with $\mu = 1$ and $\epsilon = n^2$ being locally constant (n takes different values in the fiber's core and cladding), in Minkowski spacetime and in inertial coordinates Equation (2.8) reduces to

$$(-n^2\partial_t^2 + \partial_x^2 + \partial_y^2 + \partial_z^2)A_\mu = 0. \tag{2.9}$$

2.2 Solutions for homogeneous, isotropic optical fibers with circular cross-section

In this section we review the mode solutions to Equation (2.9) for straight step-index fibers with circular cross-sections. These serve as unperturbed reference solutions to the perturbative scheme for modeling light propagation in elastically deformed fibers described in Section 2.3. Whereas the description of such modes at the level of the field strength is described in textbooks[18], the following calculation is carried out using the electromagnetic potential following Ref. 19. To distinguish the reference solution derived here from the actual solution for deformed fibers, the solutions to the unperturbed problem will be marked by a ring diacritic ($\mathring{\ }$).

The unperturbed optical fiber is modelled as a cylindrical dielectric fiber with a core of radius ρ and refractive index n_1 that is surrounded by an annular dielectric cladding of outer radius a and refractive index $n_2 < n_1$. While a is finite for the purpose of the elasticity calculations, because of the exponential decay of the electromagnetic field in the cladding we use the approximation $a = \infty$ when solving Maxwell's equations.

An efficient approach to this problem proceeds by solving Equation (2.9) in regions of constant refractive index independently and applying matching conditions at the interface. Due to the symmetry of the problem, the calculations to follow are carried out using cylindrical coordinates (t, r, θ, z). Following Ref. 19, mode solutions are obtained by decomposing the potential A_μ using the complex frame

$$e_t = \partial_t, \qquad e_\sharp = \frac{1}{\sqrt{2}}(\partial_r + \frac{\mathrm{i}}{r}\partial_\theta), \tag{2.10a}$$

$$e_z = \partial_z, \qquad e_\flat = \frac{1}{\sqrt{2}}(\partial_r - \frac{\mathrm{i}}{r}\partial_\theta), \tag{2.10b}$$

and using the ansatz

$$\mathring{A}_b = \mathring{a}_b(r)\mathrm{e}^{\mathrm{i}(\beta z + m\theta - \omega t)}, \tag{2.11}$$

so that the wave equations for the frame components $\mathring{a}_b$ decouple. Here, ω is the angular frequency of the mode, β its propagation constant, and m is the azimuthal mode index. As already mentioned, general solutions are obtained by forming wave-packets out of monochromatic solutions. In particular, dispersion can be included in the model by taking coefficients such as the refractive indices to be ω-dependent.

Writing

$$\mathring{a} = (\mathring{a}_b) \equiv (\mathring{a}_t, \quad \mathring{a}_z, \quad \mathring{a}_\sharp, \quad \mathring{a}_\flat), \tag{2.12}$$

the system (2.9) is equivalent to

$$\mathscr{H}_m \mathring{a} := (H_m \mathring{a}_t, \quad H_m \mathring{a}_z, \quad H_{m+1}\mathring{a}_\sharp, \quad H_{m-1}\mathring{a}_\flat) = 0, \tag{2.13}$$

where H_m is the Helmholtz operator

$$H_m = \frac{\partial^2}{\partial r^2} + \frac{1}{r}\frac{\partial}{\partial r} - \frac{m^2}{r^2} + n^2\omega^2 - \beta^2. \tag{2.14}$$

The requirements of regularity at the origin $r = 0$ and of exponential fall-off as $r \to \infty$ imply that solutions of (2.13) can be expressed in terms of the functions

$$f_m(c_1, c_2, r) := \begin{cases} c_1 J_m(Ur) & r < \rho, \\ c_2 K_m(Wr) & r > \rho, \end{cases} \tag{2.15}$$

where c_1 and c_2 are arbitrary constants, J_m are Bessel functions of first kind, K_m are modified Bessel functions of second kind, and the parameters U and W are defined as

$$U = \rho\sqrt{n_1^2\omega^2 - \beta^2}, \qquad W = \rho\sqrt{\beta^2 - n_2^2\omega^2}. \tag{2.16}$$

Using this notation, the relevant solutions to Equation (2.13) take the form

$$\mathring{a} = \mathscr{F}_m(\mathring{\mathbf{c}}) := (f_m(c_1, c_5, r), \quad f_m(c_2, c_6, r), \quad f_{m+1}(c_3, c_7, r), \quad f_{m-1}(c_4, c_8, r)), \tag{2.17}$$

with

$$\mathring{\mathbf{c}} = (c_1, \ldots, c_8) \tag{2.18}$$

denoting a set of constants that needs to be determined from the matching conditions at the core-cladding interface located at $r = \rho$. Specifically, we require continuity of the following field components, as discussed in Section II.D. of Ref. 19

$$\left[\!\left[\chi_{\text{gauge}}\right]\!\right] = 0, \qquad \left[\!\left[A_\mu\right]\!\right] = 0, \qquad \left[\!\left[G^{\mu\nu}\right]\!\right] n_\nu = 0, \tag{2.19}$$

in which $[\![f]\!] = (f_{\text{core}} - f_{\text{cladding}})|_{r=\rho}$ denotes the jump of a function at the core-cladding interface, and where n_μ denotes any normal to that interface (due to linearity neither the sign nor the normalization are relevant). For the ansatz (2.11) these conditions can be written concisely as $\Gamma_m[\mathring{a}] = 0$, where $\Gamma_m[\mathring{a}]$ is the eight-component vector

$$\Gamma_m[\mathring{a}] = \begin{pmatrix} [\![\mathring{a}_0]\!] \\ [\![\mathring{a}_\sharp]\!] \\ [\![\mathring{a}_\flat]\!] \\ [\![\mathring{a}_z]\!] \\ [\![n^2(\partial_r \mathring{a}_0 + \frac{\mathrm{i}\omega}{\sqrt{2}}(\mathring{a}_\sharp + \mathring{a}_\flat))]\!] \\ [\![\partial_r(\mathring{a}_\sharp - \mathring{a}_\flat) + \frac{m+1}{r}\mathring{a}_\sharp + \frac{m-1}{r}\mathring{a}_\flat]\!] \\ [\![\partial_r \mathring{a}_z]\!] \\ \left[\!\left[\mathrm{i}\omega n^2 \mathring{a}_0 + \frac{1}{\sqrt{2}}\left(\partial_r(\mathring{a}_\sharp - \mathring{a}_\flat) + \frac{m+1}{r}\mathring{a}_\sharp - \frac{m-1}{r}\mathring{a}_\flat\right)\right]\!\right] \end{pmatrix}, \tag{2.20}$$

where we kept some of the continuous terms as this simplifies the algebra later.

For solutions of the form (2.17), the interface conditions can be written in terms of matrices acting on the vector $\mathring{\mathbf{c}}$:

$$\Gamma_m[\mathring{a}] = M_m N_m \mathring{\mathbf{c}}, \tag{2.21}$$

where

$$M_m = \begin{pmatrix} 1 & 0 & 0 & 0 & -1 & 0 & 0 & 0 \\ 0 & 1 & 0 & 0 & 0 & -1 & 0 & 0 \\ 0 & 0 & \frac{m}{U} - \mathcal{J}U & 0 & 0 & 0 & \mathcal{K}W - \frac{m}{W} & 0 \\ 0 & 0 & 0 & \frac{m}{U} + \mathcal{J}U & 0 & 0 & 0 & \frac{m}{W} + \mathcal{K}W \\ \mathcal{J}n_1^2U^2 & 0 & \frac{\mathrm{i}n_1^2\omega(m - \mathcal{J}U^2)}{\sqrt{2}U} & \frac{\mathrm{i}n_1^2\omega(m + \mathcal{J}U^2)}{\sqrt{2}U} & -\mathcal{K}n_2^2W^2 & 0 & \frac{\mathrm{i}n_2^2\omega(\mathcal{K}W^2 - m)}{\sqrt{2}W} & \frac{\mathrm{i}n_2^2\omega(m + \mathcal{K}W^2)}{\sqrt{2}W} \\ 0 & 0 & U & U & 0 & 0 & W & -W \\ 0 & \mathcal{J}U^2 & 0 & 0 & 0 & -\mathcal{K}W^2 & 0 & 0 \\ \mathrm{i}n_1^2\omega & 0 & \frac{U}{\sqrt{2}} & -\frac{U}{\sqrt{2}} & -\mathrm{i}n_2^2\omega & 0 & \frac{W}{\sqrt{2}} & \frac{W}{\sqrt{2}} \end{pmatrix}, \tag{2.22}$$

with

$$\mathcal{J} = \frac{J_m'}{UJ_m}, \qquad \mathcal{K} = \frac{K_m'}{WK_m}, \tag{2.23}$$

and

$$N_m = \mathrm{diag}(J_m \quad J_m \quad J_m \quad J_m \quad K_m \quad K_m \quad K_m \quad K_m). \tag{2.24}$$

For conciseness, we suppress here the arguments of the Bessel functions, which are evaluated at the interface and read $J_m(U\rho)$ and $K_m(W\rho)$, respectively.

Non-trivial solutions $\mathring{\mathbf{c}}$ to $\Gamma_m[\mathring{a}] = 0$ exist if and only if $\det M = 0$. One can show that this determinant factorizes into a term whose roots yield physical solutions and a term whose roots correspond to gauge and ghost solutions that have either vanishing field strength $F_{\mu\nu}$ or violate the gauge condition $\chi_{\text{gauge}} = 0$[19]. The equation leading to physical solutions reads

$$(\mathcal{J}+\mathcal{K})(n_1^2\mathcal{J}+n_2^2\mathcal{K}) = m^2\frac{(U^2+W^2)^2}{U^4W^4}\frac{\beta^2}{\omega^2}, \tag{2.25}$$

where individual roots of this transcendental equation yield propagating modes. Defining the normalized frequency

$$V = \omega\rho\sqrt{n_1^2-n_2^2}, \tag{2.26}$$

and the normalized guide index b implicitly by

$$U = \sqrt{1-b}V, \qquad W = \sqrt{b}V, \tag{2.27}$$

The numerical solution to Equation (2.25) with $n_1 = 1.4712$ and $n_2 = 1.4659$ is presented in Figure 2.1, compare Ref. 18. Note in particular the shaded area in this diagram, where, for a given normalized frequency, there exist only roots for (2.25) with mode numbers $m = \pm 1$ (the curves are indifferent to the sign of m). Typical applications of single-mode fibers take place in this regime.

For a given simple root of the determinant, the kernel spans a one-dimensional subspace, leading to solutions $\mathring{\mathbf{c}}$ being determined up to an overall constant. This becomes important when one tries to define the polarization state of a superposition of simultaneously propagating solutions, as the solution vectors spanning the $m = \pm 1$-subspaces can be scaled independently[11]. In the case of single-mode fibers the $m = \pm 1$ solutions share the same root, and inspection of (2.22) shows that a change of sign for the mode number m corresponds to some sign changes and re-ordering of the entries, namely

$$\mathring{\mathbf{c}}^{-} = \begin{pmatrix} -\mathring{c}_1^{+} & \mathring{c}_2^{+} & \mathring{c}_4^{+} & \mathring{c}_3^{+} & \mathring{c}_5^{+} & \mathring{c}_6^{+} & \mathring{c}_8^{+} & \mathring{c}_7^{+} \end{pmatrix}, \tag{2.28}$$

up to a multiplicative factor that we chose to be equal to one.

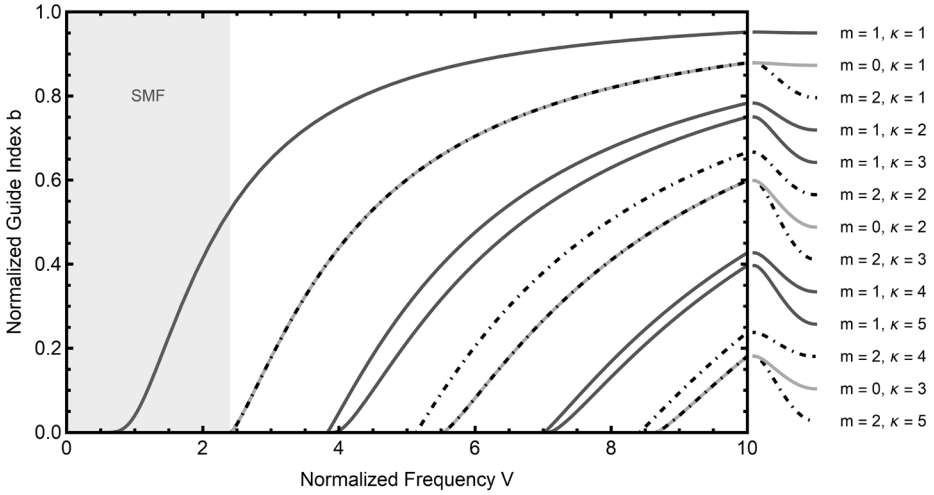

Figure 2.1. Mode diagram for an optical fiber with refractive indices $n_1 = 1.4712$ and $n_2 = 1.4659$. The parameter κ enumerates distinct roots for a fixed azimuthal mode number m. Note that in the shaded region only a single propagating mode exists for a given normalized frequency. This region corresponds to single mode optical fibers (SMF).

2.3 Multiple-scales analysis

Basing on the above description of light propagation in ideal optical fibers, in this section we derive a general formula that describes the polarization dynamics in deformed optical fibers that are invariant under translations along the fiber. This result is applied in Section 3 to compute elastically induced phase and polarization dynamics resulting from stress-induced optical inhomogeneity and anisotropy, as well as from deformations of the core-cladding interface. Denoting by $\varepsilon \ll 1$ a dimensionless expansion parameter associated to such perturbations, corrections to the field Equations (2.8) can generally be written as

$$\Box_\gamma A_\nu + \varepsilon \Sigma A_\nu = 0, \tag{2.29}$$

Here $\Box\gamma$ is the wave operator associated with the γ-metric (in regions and coordinates where the metric functions $\gamma_{\mu\nu}$ are constant, $\Box\gamma$ equals $\gamma^{\mu\nu}\partial_\mu\ \partial_\nu$, where the matrix $(\gamma^{\mu\nu})$ is the matrix inverse to the matrix $(\gamma_{\mu\nu})$. The symbol Σ denotes an operator that describes all first-order perturbations of the wave equation, which in our case arise from elasticity. Throughout, we neglect terms which are quadratic or higher-order in ε.

For our purposes there is no loss of generality in working with coordinates such that the core-cladding interface lies at $r = \rho$, as perturbed fiber geometries can be transformed to this setting by a change of coordinates (see Section 3.1 for details). This method facilitates the implementation of junction conditions at the core-cladding interface.

Restricting to the single-mode fiber solutions of Section 2.2, the $O(\varepsilon^0)$-modes have azimuthal mode number $m = \pm 1$. The remaining modes are a priori $O(\varepsilon)$. As shown in Section III.C. of Ref. 11, the propagation of these leading modes in (2.29) is governed by those Σ-terms that are isotropic (i.e., independent of θ) and those having a relative azimuthal mode number of $\Delta m = \pm 2$. Higher-order perturbation theory would allow a wider range of relative azimuthal mode numbers, since multiple combinations can again result in contributions to these leading order modes, see Refs. 11,12 for such calculations.

Consider the unperturbed single-mode solution consisting of a superposition of $m = \pm 1$ modes of the form (2.11):

$$\mathring{A} = \mathcal{A} \sum_{m=\pm 1} \mathscr{J}_m \mathscr{F}_m(\mathring{\mathbf{c}}m)\, \mathrm{e}^{\mathrm{i}(\beta z + m\theta - \omega t)}, \tag{2.30}$$

where we factored-out an overall amplitude $\mathcal{A}$, so that the coefficients $\mathscr{J}_\pm$ are normalized to $|\mathscr{J}_+|^2 + |\mathscr{J}_-|^2 = 1$. As shown in Ref. 19, the coefficients $\mathscr{J}_\pm$ can be interpreted as projections of a complex Jones vector $\mathscr{J} = \mathscr{J}_x e_x + \mathscr{J}_y e_y$, describing the polarization of the solution, onto the complex basis $e_\pm = \frac{1}{\sqrt{2}}(e_x \mp \mathrm{i} e_y)$. This translates into $\mathscr{J}_\pm = \frac{1}{\sqrt{2}}\left(\mathscr{J}_x \mp \mathrm{i}\mathscr{J}_y\right)$, and hence

$$\mathscr{J} \equiv \mathscr{J}_x e_x + \mathscr{J}_y e_y \equiv \mathscr{J}_+ e_- + \mathscr{J}_- e_+, \tag{2.31}$$

so that $\mathscr{J}_+$ and $\mathscr{J}_-$ describe, respectively, the contributions of right-handed and left-handed circular polarizations. While the fields $\mathcal{A}$ and $\mathscr{J}_m$ are constant in the unperturbed case, they satisfy propagation equations along the fiber in the perturbed case, and in fact the main aim of this work is to derive these equations in the current setting.

Following Ref. 12 we describe gradual changes in the electromagnetic field along the fiber using the multiple-scales method. This proceeds by introducing an additional length variable $\zeta = \varepsilon z$. Using z and ζ simultaneously allows separating short-distance dynamics, involving distances of the order of the optical wavelength, from that on larger length scales which are determined by the deformations of the fiber. We thus consider the following ansatz for the perturbed wave equation

$$A_b = \sum_{m=\pm 1} \left(\mathring{a}_b^m(r,\zeta) + \varepsilon \tilde{a}_b^m(r,\zeta) + O(\varepsilon^2) \right) \mathrm{e}^{\mathrm{i}(\beta z + m\theta - \omega t)}, \tag{2.32}$$

where tilde diacritics ($\tilde{\ }$) denote first-order perturbation terms. Note that the expansion above is to be understood in terms of the multiple-scales method, and *not* as a Taylor series. We will thus *not* approximate functions of ζ by $f(\zeta) = f(0) + \varepsilon z f'(0) + O(\varepsilon^2)$, see Chapter 11 of 20 for a textbook exposition.

The wave equation splits then into terms proportional to $\mathrm{e}^{\mathrm{i}(\pm 1 \pm \Delta m)\theta}$, where Δm is the relative azimuthal mode number induced by the perturbations. To describe the evolution of the polarization along the fiber it suffices to consider the terms involving $\mathrm{e}^{\pm \mathrm{i}\theta}$, leading to a coupled set of two equations

$$\mathscr{H}_+ \mathring{a}_b^+ + \varepsilon \left(\mathscr{H}_+ \tilde{a}_b^+ + 2\mathrm{i}\beta\partial_\zeta \mathring{a}_b^+ + \Sigma_b^{(+,0)}\left(\mathring{a}^+\right) + \Sigma_b^{(+,2)}\left(\mathring{a}^-\right) \right) = 0, \tag{2.33a}$$

$$\mathscr{H}_{-}\mathring{a}_b^{-}+\varepsilon\left(\mathscr{H}_{-}\tilde{a}_b^{-}+2\mathrm{i}\beta\partial_\zeta\mathring{a}_b^{-}+\sum_b^{(-,0)}(\mathring{a}^{-})+\sum_b^{(-,2)}(\mathring{a}^{+})\right)=0\,, \tag{2.33b}$$

where $\sum_b^{(\pm,\Delta m)}$ are source terms introduced by the perturbation. The current formalism allows for arbitrary such $\sum_b^{(\pm,\Delta m)}$, explicit expressions for concrete models will be considered in Section 3 below.

According to the multiple-scales method, both the leading-order terms and the ε-terms in (2.33) must vanish. It follows from the analysis of the unperturbed problem that the zero-order solutions take the form

$$\mathring{a}^{\pm}=\mathscr{J}_{\pm}(\zeta)\mathscr{F}_{\pm}(\mathring{\mathfrak{c}}^{\pm})\,, \tag{2.34}$$

which generalize the unperturbed solutions in (2.17) by allowing for a Jones vector $\mathscr{J}$ that depends on ζ. Its components $\mathscr{J}_{\pm}(\zeta)$ will be determined by the equations, as follows: The ε-part of (2.33) is a Helmholtz equation for $\tilde{a}_b^{\pm}$ with known source terms

$$\mathscr{H}_{\pm}\tilde{a}_b^{\pm}=-2\mathrm{i}\beta\partial_\zeta\mathring{a}_b^{\pm}-\sum_b^{(\pm,0)}(\mathring{a}^{\pm})-\sum_b^{(\pm,2)}(\mathring{a}^{\mp})\,, \tag{2.35}$$

whose solutions are given by

$$\tilde{a}^{\pm}=\mathscr{F}_{\pm}(\tilde{\mathfrak{c}}^{\pm})-\mathscr{G}_{\pm}\left(2\mathrm{i}\beta\partial_\zeta\mathring{a}_b^{\pm}+\sum_b^{(\pm,0)}(\mathring{a}^{\pm})+\sum_b^{(\pm,2)}(\mathring{a}^{\mp})\right), \tag{2.36}$$

where $\mathscr{G}_{\pm}=\mathscr{G}_{\pm 1}$ is a multi-component operator[12]

$$\mathscr{G}_m(f)=\big(G_m(f),\quad G_m(f),\quad G_{m+1}(f),\quad G_{m-1}(f)\big)\,, \tag{2.37}$$

in which $G_m(f)$ is the Green's operator for the Helmholtz equation

$$G_m(f):=\begin{cases}\dfrac{\pi}{2}Y_m(Ur)\displaystyle\int_0^r J_m(Us)f(s)s\,\mathrm{d}s+\dfrac{\pi}{2}J_m(Ur)\int_r^\rho Y_m(Us)f(s)s\,\mathrm{d}s & r<\rho,\\ -I_m(Wr)\displaystyle\int_r^\infty K_m(Ws)f(s)s\,\mathrm{d}s-K_m(Wr)\int_\rho^r I_m(Ws)f(s)s\,\mathrm{d}s & r>\rho.\end{cases} \tag{2.38}$$

Here the Y_m's are Bessel functions of the second kind, and I_m's are modified Bessel functions of the first kind.

Equation (2.36) solves the field equations in the core and cladding separately. To obtain a solution that is valid throughout the waveguide the field must satisfy the interface conditions given in Equation (2.19). In the perturbed case these can now contain functions of order ε which depend upon the radial and angular coordinates and the unperturbed solutions $\mathring{a}^{\pm}$. Following the reasoning leading to (2.33) we again restrict to isotropic and quadrupole perturbations, i.e., angular dependence $\Delta m=\{0,\pm 2\}$, yielding the perturbed interface conditions

$$\Gamma_{\pm}(\tilde{a}^{\pm})+\tilde{\Gamma}^{(\pm,0)}(\mathring{a}^{\pm})+\tilde{\Gamma}^{(\pm,2)}(\mathring{a}^{\mp})=0\,. \tag{2.39}$$

Here $\Gamma_{\pm}$ is given in Equation (2.20), while $\tilde{\Gamma}^{(\pm,\Delta m)}$ are the correction terms specific to the perturbations under consideration and will be determined in Section 3.

These can be written using (2.36) as

$$M^{\pm}N^{\pm}\tilde{\mathfrak{c}}^{\pm}=\Gamma_{\pm 1}\left[\mathscr{G}_{\pm}\left(2\mathrm{i}\beta\partial_\zeta\mathring{a}_b^{\pm}+\sum_b^{(\pm,0)}(\mathring{a}^{\pm})+\sum_b^{(\pm,2)}(\mathring{a}^{\mp})\right)\right]-\tilde{\Gamma}^{(\pm,0)}(\mathring{a}^{\pm})-\tilde{\Gamma}^{(\pm,2)}(\mathring{a}^{\mp})\,, \tag{2.40}$$

where $M^{\pm}=M_{\pm 1}$ and $N^{\pm}=N_{\pm 1}$ are given by Equation (2.22) and Equation (2.24). Since $M^{\pm}$ is singular due to the dispersion relation, the vectors given by the right-hand side of Equation (2.40) have to lie in the image of $M^{\pm}$. An explicit calculation shows that the cokernel of $M^{\pm}$ is one-dimensional. Let us denote by $\xi_{\pm}$ some basis vectors of the cokernel of $M^{\pm}$:

$$\xi_{+}M^{+}=0,\qquad\qquad \xi_{-}M^{-}=0. \tag{2.41}$$

Then Equation (2.40) admits solutions if and only if

$$\xi_{\pm}\Gamma_{\pm}\left[\mathscr{G}_{\pm}\left(2\mathrm{i}\beta\frac{\partial\mathring{a}_b^{\pm}}{\partial\zeta}+\Sigma_b^{(\pm,0)}(\mathring{a}^{\pm})+\Sigma_b^{(\pm,2)}(\mathring{a}^{\mp})\right)\right]-\xi_{\pm}\tilde{\Gamma}^{(\pm,0)}(\mathring{a}^{\pm})-\xi_{\pm}\tilde{\Gamma}^{(\pm,2)}(\mathring{a}^{\pm})=0. \tag{2.42}$$

Since $\mathring{a}_b^+$ and $\mathring{a}_b^-$ depend on the coefficients $\mathscr{J}_+$ and $\mathscr{J}_-$, respectively, this equation provides the desired propagation law for the Jones vector. Indeed, inserting (2.34) one obtains

$$\frac{\mathrm{d}}{\mathrm{d}\zeta}\begin{pmatrix}\mathscr{J}_+\\ \mathscr{J}_-\end{pmatrix}=\mathrm{i}\mathcal{M}\begin{pmatrix}\mathscr{J}_+\\ \mathscr{J}_-\end{pmatrix}, \tag{2.43}$$

where

$$\begin{aligned}\mathcal{M}&\equiv\begin{pmatrix}\mathcal{M}_+^{\ +} & \mathcal{M}_+^{\ -}\\ \mathcal{M}_-^{\ +} & \mathcal{M}_-^{\ -}\end{pmatrix}\\ &=\frac{1}{2\beta}\begin{pmatrix}\dfrac{\xi_+\left[\Gamma_+\mathscr{G}_+\Sigma^{(+,0)}(\mathscr{F}_+)-\tilde{\Gamma}^{(+,0)}(\mathscr{F}_+)\right]}{\xi_+\Gamma_+\mathscr{G}_+(\mathscr{F}_+)} & \dfrac{\xi_+\left[\Gamma_+\mathscr{G}_+\Sigma^{(+,2)}(\mathscr{F}_-)-\tilde{\Gamma}^{(+,2)}(\mathscr{F}_-)\right]}{\xi_+\Gamma_+\mathscr{G}_+(\mathscr{F}_+)}\\ \dfrac{\xi_-\left[\Gamma_-\mathscr{G}_-\Sigma^{(-,2)}(\mathscr{F}_+)-\tilde{\Gamma}^{(-,2)}(\mathscr{F}_+)\right]}{\xi_-\Gamma_-\mathscr{G}_-(\mathscr{F}_-)} & \dfrac{\xi_-\left[\Gamma_-\mathscr{G}_-\Sigma^{(-,0)}(\mathscr{F}_-)-\tilde{\Gamma}^{(-,0)}(\mathscr{F}_-)\right]}{\xi_-\Gamma_-\mathscr{G}_-(\mathscr{F}_-)}\end{pmatrix},\end{aligned} \tag{2.44}$$

where $\mathscr{F}_+\equiv\mathscr{F}_+(\mathring{\mathbf{c}}^+)$ and $\mathscr{F}_-\equiv\mathscr{F}_-(\mathring{\mathbf{c}}^-)$. The Cartesian components of the Jones vector thus satisfy

$$\frac{\mathrm{d}}{\mathrm{d}\zeta}\begin{pmatrix}\mathscr{J}_x\\ \mathscr{J}_y\end{pmatrix}=\mathrm{i}\hat{\mathcal{M}}\begin{pmatrix}\mathscr{J}_x\\ \mathscr{J}_y\end{pmatrix}, \tag{2.45}$$

where $\hat{\mathcal{M}}$ can be decomposed in terms of the four Pauli matrices as

$$\begin{aligned}\hat{\mathcal{M}}=&\frac{1}{2}(\mathcal{M}_+^{\ +}+\mathcal{M}_-^{\ -})\sigma_0+\frac{\mathrm{i}}{2}(\mathcal{M}_+^{\ -}+\mathcal{M}_-^{\ +})\sigma_1\\ &+\frac{1}{2}(\mathcal{M}_+^{\ +}-\mathcal{M}_-^{\ -})\sigma_2+\frac{1}{2}(\mathcal{M}_+^{\ -}+\mathcal{M}_-^{\ +})\sigma_3.\end{aligned} \tag{2.46}$$

In all cases below one has $\mathcal{M}_+^{\ +}=\mathcal{M}_-^{\ -}$ and $\mathcal{M}_+^{\ -}=\mathcal{M}_-^{\ +}$, so that $\hat{\mathcal{M}}$ takes to the form

$$\hat{\mathcal{M}}=\mathcal{M}_+^{\ +}\begin{pmatrix}1&0\\0&1\end{pmatrix}+\mathcal{M}_+^{\ -}\begin{pmatrix}1&0\\0&-1\end{pmatrix}. \tag{2.47}$$

In this case, the diagonal components of $\mathcal{M}$ (which arise from perturbations with $\Delta m = 0$) thus describe phase shifts, as they produce the same effect on $\mathscr{J}_x$ and $\mathscr{J}_y$, while off-diagonal components of $\mathcal{M}$ (corresponding to $\Delta m = \pm 2$) describe birefringence, producing opposite phase shifts on $\mathscr{J}_x$ and $\mathscr{J}_y$.

3 Elasticity

To continue, we wish to determine the source terms $\Sigma^{(\pm,0)}$ and $\Sigma^{(\pm,2)}$ arising from elastic perturbations of the fiber, after which (2.44) can be evaluated numerically.

For this we consider elastic deformations of the optical fibers resulting from ambient pressure, temperature, and gravity acting as a body force orthogonal to the principal axis of the fiber. Considering a circular optical fiber as described in Section 2.2, we take the elastic parameters of the core and cladding to be identical and constant throughout the medium, resulting in a simple model of a homogeneous and isotropic cylinder of length L and radius a.

In this section we use Euclidean coordinates (x, y, z) in which the fiber is aligned along the z-axis, with $r = \sqrt{x^2+y^2}$ and with $(x, y) = (r\ cos(\theta), r\ sin(\theta))$. In the remainder of this work we restrict the analysis to linear elasticity. We recall here the main equations, referring for a more detailed treatment to Ref. 7. The displacement field u_i describes small deformations of the material and determines the strain tensor, which we denote by u_{ij}, via

$$u_{ij}=\frac{1}{2}(\partial_i u_j+\partial_j u_i). \tag{3.1}$$

The strain is related to the material stress σ_{ij} via the generalized Hooke law for isotropic media[21,22], as extended to account for changes of temperature $T - T_0$. Assuming the material to be thermally-linear and thermally-isotropic one has[22]

$$\sigma_{ij} = \lambda u_{kk}\,\delta_{ij} + 2\mu u_{ij} - (3\lambda + 2\mu)\alpha(T - T_0)\delta_{ij}, \tag{3.2}$$

where λ and μ are Lamé's first and second parameters of the material, and where α is the coefficient of thermal expansion, all taken to be constant throughout the waveguide. The second Lamé parameter μ is also referred to as the shear modulus, $\nu = \lambda/[2(\lambda + \mu)]$ is known as the Poisson ratio, and the Young modulus is given by $E = 2\mu(1 + \nu)$. Material parameters for fused silica, which is widely used in optical fibers, are listed in Table 3.1.

Static configurations are described by solutions to the equilibrium equations[22]

$$\partial_j \sigma_{ij} + F_i = 0, \tag{3.3}$$

with $F_i = -\partial_i V$ denoting the gravitational body force, where $V = \mathrm{g}\rho y$ is the gravitational potential, with ρ being the mass density of the material and g the gravitational acceleration of Earth. At the object's surface, one has the traction boundary conditions[21]

$$\sigma_{ij} n_j = P_i, \tag{3.4}$$

where n_j is the outward-pointing unit normal vector of the material surface and P_i is the external pressure.

Taking into account the translational symmetry along the fiber, as well as the fact that the radius a of the fiber is significantly smaller than its length L, $a \ll L$, the calculations can be reduced to those on two-dimensional cross-sections orthogonal to the main axis. The textbook approach does so by setting the out-of-plane strain components to zero [22, Chapter 7] leading to algebraic expressions for the out-of-plane stress and two-dimensional equilibrium Equations (3.3). This can be generalized by allowing for a linear displacement along the fiber (cf. 23)

$$u_z = \kappa z, \tag{3.5}$$

where κ is a constant, implying

$$u_{xz} = u_{yz} = 0, \qquad \text{and} \qquad u_{zz} = \kappa. \tag{3.6}$$

The equilibrium equations can now be solved by introducing a stress function ϕ, related to the stress tensor in cylindrical frame components via

$$\sigma_{rr} = \frac{1}{r}\partial_r\phi + \frac{1}{r^2}\partial_\theta^2\phi + V, \qquad \sigma_{r\theta} = \partial_r^2\phi + V, \qquad \sigma_{\theta\theta} = -\partial_r\left(\frac{1}{r}\partial_\theta\phi\right). \tag{3.7}$$

The general solution to these equations has been written down by Michell[24]. Assuming regularity, vertical reflection symmetry, and absence of friction at the fiber's boundary one is led to[7]

$$\phi(r,\theta) = d_0 r^2 + \sum_{\ell\geq 2}\left(1 + \frac{1-\ell}{1+\ell}\frac{r^2}{a^2}\right) b_\ell r^\ell \cos\left[\ell\left(\theta + \frac{\pi}{2}\right)\right], \tag{3.8}$$

Table 3.1. Properties of silica oxide glass from Ref. 25.

Poisson ratio ν	0.17
Young modulus E	73.1 GPa
Mass density ρ	2.2 g cm^{-3}
Thermal expansion coefficient α	5.5 x 10^{-7} K^{-1}

where the angle θ used here has been shifted by $\pi/2$ relative to that in 7 to measure the usual angle from the horizontal. The parameters d_0 and b_ℓ are determined by the boundary condition (3.4). Combining (3.2) and (3.7) yields a parameterized expression for the strain tensor,

$$u_{rr} = -\frac{1}{2\mu}\Bigg\{-(1-2\nu)\,g r\rho\sin(\theta) - 2(1-2\nu)\,d_0 + 2\mu\nu\kappa - 2\mu(1+\nu)\,\alpha(T-T_0) \\ -\sum_{\ell=2}^{\infty}\left[\ell - (\ell-2+4\nu)\frac{r^2}{a^2}\right](1-\ell)\,r^{\ell-2}b_\ell\cos\left[\ell\left(\theta+\frac{\pi}{2}\right)\right]\Bigg\}, \tag{3.9a}$$

$$u_{r\theta} = -\frac{1}{2\mu}\sum_{\ell=2}^{\infty}\left[1-\frac{r^2}{a^2}\right](1-\ell)\,\ell\,r^{\ell-2}b_\ell\sin\left[\ell\left(\theta+\frac{\pi}{2}\right)\right], \tag{3.9b}$$

$$u_{\theta\theta} = -\frac{1}{2\mu}\Bigg\{-(1-2\nu)\,g r\rho\sin(\theta) - 2(1-2\nu)\,d_0 + 2\mu\nu\kappa - 2\mu(1+\nu)\,\alpha(T-T_0) \\ +\sum_{\ell=2}^{\infty}\left[\ell - (\ell+2-4\nu)\frac{r^2}{a^2}\right](1-\ell)\,r^{\ell-2}b_\ell\cos\left[\ell\left(\theta+\frac{\pi}{2}\right)\right]\Bigg\}. \tag{3.9c}$$

This can be integrated using (3.1), leading to the following form of the frame-components of the displacement vector:

$$u_r(r,\theta) = \mu^{-1}(1-2\nu)\,d_0 r - \nu\kappa r + (1+\nu)\,\alpha r(T-T_0) \\ +\frac{1}{2\mu}\Bigg\{\left[\frac{1}{2}g\rho(1-2\nu)r^2 + 2\mu\Xi\right]\sin(\theta) \\ -\sum_{\ell\geq 2}\left[\ell - (2-4\nu-\ell)\frac{1-\ell}{1+\ell}\frac{r^2}{a^2}\right]b_\ell r^{\ell-1}\cos\left[\ell\left(\theta+\frac{\pi}{2}\right)\right]\Bigg\}, \tag{3.10a}$$

$$u_\theta(r,\theta) = \frac{1}{2\mu}\Bigg\{\left[-\frac{1}{2}g\rho(1-2\nu)r^2 + 2\mu\Xi\right]\cos(\theta) \\ +\sum_{\ell\geq 2}\left[\ell + (4-4\nu+\ell)\frac{1-\ell}{1+\ell}\frac{r^2}{a^2}\right]b_\ell r^{\ell-1}\sin\left[\ell\left(\theta+\frac{\pi}{2}\right)\right]\Bigg\}. \tag{3.10b}$$

The parameter Ξ describes rigid vertical displacements of the fiber and can thus be determined, for example, by prescribing the displacement at a point of the fiber's boundary, e.g., by setting $u_r(a, -\frac{\pi}{2}) = u_\theta(a, -\frac{\pi}{2}) = 0$.

Anticipating, the only expansion coefficients of the Michell solution that couple to the optical phase and polarization are d_0 and b_2. It is worth noting that these two coefficients are completely determined by the strain tensor at the axis of the fiber. Indeed, in Cartesian coordinates we have

$$(u_{xx} + u_{yy})\big|_{r=0} = 2\mu^{-1}(1-2\nu)d_0 - 2\nu\kappa + 2(1+\nu)\,\alpha(T-T_0), \tag{3.11a}$$

$$(u_{xx} - u_{yy})\big|_{r=0} = -2\mu^{-1}b_2. \tag{3.11b}$$

In Ref. 7 a number of physically motivated boundary conditions were considered. For the numerics of Section 3.3 we restrict ourselves to the model discussed in Ref. [7, Section 4.2.1], namely the waveguide resting on a rigid plane with an extended contact region. In this case one has

$$d_0 = -\frac{1}{4}(ag\rho + 2\mathfrak{p}), \qquad b_\ell = \frac{g\rho}{2a^{\ell-3}(\ell-1)}, \quad \ell\geq 2, \tag{3.12}$$

where $\mathfrak{p}$ is an ambient isotropic pressure.

The following Section 3.1 and Section 3.2 describe the influence of such fiber deformations on the electromagnetic modes propagating therein.

3.1 Displacement

Transverse deformations of an optical fiber which are invariant under translation along its axis are described by displacements of the form

$$r \to r + u_r(r,\theta), \qquad \theta \to \theta + u_\theta(r,\theta)/r, \tag{3.13}$$

which is assumed to be sufficiently small so that nonlinear terms in u_r and u_θ are negligible.

The deformation implies that the core-cladding interface is displaced from its reference location, while the calculations in Section 2.3 require the core-cladding interface to lie at a constant radial coordinate distance from the fiber's axis. This can be resolved by performing a coordinate transformation, namely the inverse of (3.13), so that the core-cladding interface is again located at $r = \rho$ in the new coordinates. This coordinate transformation results in additional source terms in the field equations as well as the interface equations.

The details are as follows.

3.1.1 The equations. For definiteness let

$$(x^\mu) \equiv (t,\vec{x}) \equiv (t,x^i) \equiv (t,x,y,z) \tag{3.14}$$

denote the coordinates before the waveguide has been deformed, and let $(\overline{x}^\mu) \equiv (t,\overline{x}^i) \equiv (t,\overline{x},\overline{y},\overline{z})$ describe the deformed configuration:

$$\overline{x}^i = x^i + u^i(\vec{x}). \tag{3.15}$$

The interface between the core and the cladding is located at $x^2 + y^2 = \rho^2$.

To avoid ambiguities: the barred coordinates are the original lab coordinates, in which the core-cladding interface is *not* at $\overline{r} \equiv \sqrt{\overline{x}^2 + \overline{y}^2} = \rho$ in general; all barred objects refer to this coordinate system. We transition to the unbarred coordinate system, adapted to the deformation of the waveguide, in a way so that the core-cladding interface lies at $r = \sqrt{x^2+y^2}=\rho$.

We assume that u^i and its derivatives are of order ε, where ε is small compared to the remaining scales involved. In particular the map $x^i \mapsto \overline{x}^i$ is invertible with

$$x^i = \overline{x}^i + O(\varepsilon), \qquad x^i = \overline{x}^i - u^i\big|_{x^j=\overline{x}^j} + O(\varepsilon^2). \tag{3.16}$$

Denoting by $\overline{A}_\mu$ the full vector potential in the barred coordinate system,

$$\overline{A}_\mu(t,\overline{x},\overline{y},\overline{z})\big|_{\overline{x}^i = x^i + u^i(\vec{x})} = A_\nu(t,\vec{x})\frac{\partial x^\nu}{\partial \overline{x}^\mu}, \tag{3.17}$$

one has

$$\overline{A}_0 = A_0 - \frac{\partial A_0}{\partial x^i}u^i + O(\varepsilon^2), \quad \overline{A}_i = A_i - \frac{\partial A_i}{\partial x^j}u^j - A_j\frac{\partial u^j}{\partial x^i} + O(\varepsilon^2). \tag{3.18}$$

We emphasize that both A_μ and $\overline{A}_\mu$ refer to the full vector potential, each consisting of an unperturbed part and perturbations.

Away from the interface the vector potential $\overline{A}_\mu$ satisfies the wave equation

$$(-n^2\partial_t^2 + \partial_{\overline{x}}^2 + \partial_{\overline{y}}^2 + \partial_{\overline{z}}^2)\overline{A}_\mu = 0. \tag{3.19}$$

In the x^μ-coordinates this becomes

$$(-n^2\partial_t^2 + g^{ij}\nabla_i\nabla_j)A_\mu = 0, \tag{3.20}$$

where g^{ij} is the space-part of the transformed contravariant metric

$$g^{\mu\nu}(t,x,y,z)=\left(\overline{g}^{\alpha\beta}\frac{\partial x^{\mu}}{\partial\overline{x}^{\alpha}}\frac{\partial x^{\nu}}{\partial\overline{x}^{\beta}}\right)\Bigg|_{\overline{x}^{i}=x^{i}+u^{i}(\vec{x})}\equiv\left(\eta^{\alpha\beta}\frac{\partial x^{\mu}}{\partial\overline{x}^{\alpha}}\frac{\partial x^{\nu}}{\partial\overline{x}^{\beta}}\right)\Bigg|_{\overline{x}^{i}=x^{i}+u^{i}(\vec{x})},\tag{3.21}$$

with ∇_{μ} denoting the covariant derivative of the transformed metric. In particular, keeping in mind that the $\overline{x}^{i}$'s are Euclidean coordinates in which $\overline{g}^{ij}=\delta^{ij}=\delta_{ij}$ where δ^{i}_{j} is the Kronecker delta,

$$g^{ij}(x,y,z)=\left(\delta^{k\ell}\frac{\partial x^{i}}{\partial\overline{x}^{k}}\frac{\partial x^{j}}{\partial\overline{x}^{\ell}}\right)\Bigg|_{\overline{x}^{i}=x^{i}+u^{i}(\vec{x})}=\delta^{ij}-\partial_{i}u^{j}-\partial_{j}u^{i}+O(\varepsilon^{2})=\delta^{ij}+O(\varepsilon).\tag{3.22}$$

The Christoffel symbols are

$$\Gamma^{0}_{\alpha\beta}=\Gamma^{\alpha}_{0\beta}=0,\qquad\qquad\Gamma^{i}_{jk}=\partial_{j}\partial_{k}u^{i}+O(\varepsilon^{2})=O(\varepsilon),\tag{3.23}$$

so that

$$\nabla_{0}A_{0}=\partial_{t}A_{0},\qquad\nabla_{i}A_{0}=\partial_{i}A_{0},\qquad\nabla_{i}\nabla_{j}A_{0}=\partial_{i}\partial_{j}A_{0}-(\partial_{i}\partial_{j}u^{k})\partial_{k}A_{0}+O(\varepsilon^{2}),\tag{3.24a}$$

$$\nabla_{0}A_{i}=\partial_{t}A_{i},\quad\nabla_{j}A_{k}=\partial_{j}A_{k}-A_{\ell}\partial_{j}\partial_{k}u^{\ell}+O(\varepsilon^{2}),\tag{3.24b}$$

$$\nabla_{i}\nabla_{j}A_{k}=\partial_{i}(\partial_{j}A_{k}-A_{\ell}\partial_{j}\partial_{k}u^{\ell})-\partial_{i}\partial_{j}u^{\ell}\partial_{\ell}A_{k}-\partial_{i}\partial_{k}u^{\ell}\partial_{j}A_{\ell}+O(\varepsilon^{2}),\tag{3.24c}$$

Hence, up to terms of order ε^{2}, the system (3.20) can be rewritten as

$$(-n^{2}\partial_{t}^{2}+\delta^{ij}\partial_{i}\partial_{j})A_{0}=\delta^{ij}\left[2\partial_{i}u^{\ell}\partial_{j}\partial_{\ell}A_{0}+\partial_{i}\partial_{j}u^{\ell}\partial_{\ell}A_{0}\right],\tag{3.25a}$$

$$(-n^{2}\partial_{t}^{2}+\delta^{ij}\partial_{i}\partial_{j})A_{k}=\delta^{ij}\left[2\partial_{i}u^{\ell}\partial_{j}\partial_{\ell}A_{k}+\partial_{i}\partial_{j}u^{\ell}\partial_{\ell}A_{k}+2\partial_{i}\partial_{k}u^{\ell}\partial_{j}A_{\ell}+A_{\ell}\partial_{i}\partial_{j}\partial_{k}u^{\ell}\right].\tag{3.25b}$$

3.1.2 Boundary conditions. Let n^{i} denote the field of normals to the interface between the core and the cladding. In the unbarred coordinate system the interface is located at $r\equiv\sqrt{x^{2}+y^{2}}=\rho$, where $\vec{x}$ denotes the position vector in the plane perpendicular to the axis of the fiber. The covariant components of the normal n_{A}, $A=1,2$, are proportional to x^{A}/r, say $n_{A}=\alpha x^{A}/r$. As already mentioned above, the normalization of n_{A} is irrelevant for the equations, and thus we take

$$n_{A}=\frac{x^{A}}{r}+O(\varepsilon^{2}),\qquad\qquad n_{z}=0.\tag{3.26}$$

The general form of the junction conditions depends neither on the details of the constitutive tensor nor on the coordinates in which they are written, as they are generally covariant. As a consequence, the continuity conditions at the core-cladding interface take the same form as in Eq. (2.19), reproduced here for the convenience of the reader

$$[\![\chi_{\text{gauge}}]\!]=0,\qquad\qquad[\![A_{\mu}]\!]=0,\qquad\qquad[\![G^{\mu\nu}]\!]n_{\nu}=0,\tag{3.27}$$

with

$$(n_{\mu}):=(n_{0},n_{i})\equiv(n_{t},n_{i})=(0,n_{1},n_{2},0).$$

Here, as above, $[\![f]\!]=(f_{\text{core}}-f_{\text{cladding}})|_{r=\rho}$ denotes the jump of a function f at the surface where $r^{2}=x^{2}+y^{2}$ equals ρ^{2}.

To continue, we need explicit formulae for $G^{\mu\nu}n_{\nu}$. Keeping in mind our assumption that $\mu=1$, we have

$$\begin{aligned}G^{tA}n_{A}=G^{tr}&=\gamma^{tt}\gamma^{r\nu}(\partial_{t}A_{\nu}-\partial_{\nu}A_{t})\\&=-n^{2}(1-2\partial_{r}u_{r})(\partial_{t}A_{r}-\partial_{r}A_{t})-n^{2}r^{-2}(u_{\theta}-\partial_{\theta}u_{r}-r\partial_{r}u_{\theta})(\partial_{t}A_{\theta}-\partial_{\theta}A_{t})+O(\varepsilon^{2}),\end{aligned}\tag{3.28a}$$

$$G^{rA}n_{A}=G^{rr}=0,\tag{3.28b}$$

$$G^{\theta A}n_A = G^{\theta r} = \gamma^{\theta r}\gamma^{r\theta}(\partial_r A_\theta - \partial_\theta A_r) + \gamma^{\theta\theta}\gamma^{rr}(\partial_\theta A_r - \partial_r A_\theta)$$
$$= r^{-2}\left[1 - 2r^{-1}(u_r + \partial_\theta u_\theta + \frac{1}{2}r\partial_r u_r)\right](\partial_\theta A_r - \partial_r A_\theta) + O(\varepsilon^2), \tag{3.28c}$$

$$G^{zA}n_A = G^{zr} = \gamma^{zz}\gamma^{r\nu}\left(\partial_z A_\nu - \partial_\nu A_z\right)$$
$$= \left(1 - 2\partial_r u_r\right)\left(\partial_z A_r - \partial_r A_z\right) + r^{-2}\left(u_\theta - \partial_\theta u_r - r\partial_r u_\theta\right)\left(\partial_z A_\theta - \partial_\theta A_z\right) + O\left(\varepsilon^2\right). \tag{3.28d}$$

Thus, using $[\![A_\mu]\!] = 0$, we obtain

$$[\![G^{t\nu}n_\nu]\!] = -\left(\frac{x^B}{r} - \partial_r u^B - \partial_B u^r\right)[\![n^2(\partial_t A_B - \partial_B A_t)]\!] + O(\varepsilon^2), \tag{3.29a}$$

$$[\![G^{r\nu}n_\nu]\!] = [\![G^{rr}]\!] + O(\varepsilon^2) = O(\varepsilon^2), \tag{3.29b}$$

$$[\![G^{\theta\nu}n_\nu]\!] = r^{-2}\left[1 - 2r^{-1}(u_r + \partial_\theta u_\theta + \frac{1}{2}r\partial_r u_r)\right][\![\partial_r A_\theta]\!] + O(\varepsilon^2), \tag{3.29c}$$

$$[\![G^{z\nu}n_\nu]\!] = \left(1 - 2\partial_r u^r\right)[\![\partial_r A_z]\!] + O(\varepsilon^2), \tag{3.29d}$$

and

$$[\![\chi_{\text{gauge}}]\!] = [\![-n^2\partial_t A_0 + \left(1 - 2\partial_r u_r\right)\partial_r A_r + r^{-2}(u_\theta - \partial_\theta u_r - r\partial_r u_\theta)\partial_r A_\theta]\!] + O(\varepsilon^2). \tag{3.30}$$

3.1.3 Explicit expressions. As already pointed-out in Section 2.3, the results obtained from first-order perturbation theory only depend on perturbation terms with relative azimuthal mode number $\Delta m \in \{0, +2, -2\}$, i.e., only terms without angular dependence or terms proportional to $e^{\pm 2i\theta}$. We treat these cases independently in the following paragraphs.

Radial perturbations In the simplest case $\Delta m = 0$ the perturbative terms are independent of the angular coordinate θ, and we can write the wave equation again in terms of Helmholtz operators

$$(\mathscr{H}_m + \varepsilon\delta\mathscr{H}_m)a_b = 0. \tag{3.31}$$

Explicitly, for the displacements given in (3.13) together with (3.10) one finds

$$\varepsilon\delta\mathscr{H}_m = -2(\mu^{-1}(1-2\nu)d_0 - \nu\kappa + (1+\nu)\alpha(T - T_0))(n^2\omega^2 - \beta^2). \tag{3.32}$$

This is equivalent to the unperturbed Equation (2.13) with rescaled frequency and wave vector. Consequently, the solutions are given as in (2.15)–(2.17) with the substitutions

$$U \to \left[1 - (1-2\nu)d_0/\mu + \nu\kappa - (1+\nu)\alpha\left(T - T_0\right)\right]U, \tag{3.33a}$$

$$W \to [1 - (1-2\nu)d_0/\mu + \nu\kappa - (1+\nu)\alpha(T - T_0)]W. \tag{3.33b}$$

This, in turn, introduces a shift in the roots of (2.25) and thus a perturbation of β, namely

$$\frac{\delta\beta}{\beta} = [(1-2\nu)d_0/\mu - \nu\kappa + (1+\nu)\alpha(T - T_0)]V\frac{n_1^2 - n_2^2}{2\bar{n}^2}\frac{\mathrm{d}b}{\mathrm{d}V}, \tag{3.34}$$

where $\bar{n} = \beta/w = \sqrt{bn_1^2 + (1-b)n_2^2}$ is the effective refractive index, and $\mathrm{d}b/\mathrm{d}V$ is the derivative of the normalized guide index with respect to the normalized frequency, which can be read from Figure 2.1.

Alternatively, in the current simple case one can directly work in the original coordinates, with $\delta\mathscr{H}_m = 0$ in (3.32). The interface region is then displaced as $\rho \to \rho + u_r(\rho)$. Such a perturbation in Equation (2.16) is equivalent to (3.34).

Perturbations with angular dependence Apart from the angle-independent terms described above, the displacements given in Equation (3.10) lead to correction terms to the field equations with angular dependence $\mathrm{e}^{\pm 2\mathrm{i}\theta}$ that can be written in the form of Equation (2.33) with

$$\varepsilon\sum_{t}^{(\pm,2)} = \frac{b_2}{\mu r^2 a^2}\Big[(a^2+2(1-\nu)r^2)\mathring{a}_t^{\mp} - r(a^2-2r^2(1+\nu))\partial_r\,\mathring{a}_t^{\mp} - r^2(a^2-2r^2\nu)\partial_r^2\,\mathring{a}_t^{\mp}\Big], \tag{3.35a}$$

$$\varepsilon\sum_{z}^{(\pm,2)} = \frac{b_2}{\mu r^2 a^2}\Big[(a^2+2(1-\nu)r^2)\mathring{a}_z^{\mp} - r(a^2-2r^2(1+\nu))\partial_r\,\mathring{a}_z^{\mp} - r^2(a^2-2r^2\nu)\partial_r^2\,\mathring{a}_z^{\mp}\Big], \tag{3.35b}$$

$$\varepsilon\sum_{\sharp}^{(+,2)} = \frac{b_2}{\mu r a^2}\Big[(a^2+2r^2(1+\nu))\partial_r\,\mathring{a}_{\sharp}^{-} - r(a^2-2r^2\nu))\partial_r^2\,\mathring{a}_{\sharp}^{-}\Big], \tag{3.35c}$$

$$\varepsilon\sum_{\flat}^{(-,2)} = \frac{b_2}{\mu r a^2}\Big[(a^2+2r^2(1+\nu))\partial_r\,\mathring{a}_{\flat}^{+} - r(a^2-2r^2\nu))\partial_r^2\,\mathring{a}_{\flat}^{+}\Big], \tag{3.35d}$$

$$\varepsilon\sum_{\flat}^{(+,2)} = \frac{b_2}{\mu r a^2}\Big[2r(-2+4\nu)\mathring{a}_{\flat}^{-} - (3a^2+2r^2(1-5\nu))\partial_r\,\mathring{a}_{\flat}^{-} - r\Big(a^2-2r^2\nu\Big)\partial_r^2\,\mathring{a}_{\flat}^{-} + 4r\,\mathring{a}_{\sharp}^{-} + 4r^2\partial_r\,\mathring{a}_{\sharp}^{-}\Big], \tag{3.35e}$$

$$\varepsilon\sum_{\sharp}^{(-,2)} = \frac{b_2}{\mu r a^2}\Big[2r(-2+4\nu)\mathring{a}_{\sharp}^{+} - (3a^2+2r^2(1-5\nu))\partial_r\,\mathring{a}_{\sharp}^{+} - r\Big(a^2-2r^2\nu\Big)\partial_r^2\,\mathring{a}_{\sharp}^{+} + 4r\,\mathring{a}_{\flat}^{+} + 4r^2\partial_r\,\mathring{a}_{\flat}^{+}\Big]. \tag{3.35f}$$

For the correction terms arising for the interface conditions (2.39) we find explicitly

$$\tilde{\Gamma}^{(\pm,2)}[\mathring{a}^{\mp}] = \mathrm{i}b_2\mu^{-1}\begin{pmatrix} 0\\0\\0\\0\\ \pm\left(1-\dfrac{\rho^2}{a^2}\right)\Big[\!\Big[\, n^2\left(\mp\mathrm{i}r^{-1}\,\mathring{a}_t^{\mp} - \dfrac{1}{\sqrt{2}}\omega\,\mathring{a}_{\sharp}^{\mp} + \dfrac{1}{\sqrt{2}}\omega\,\mathring{a}_{\flat}^{\mp}\right)\Big]\!\Big]\\ 0\\0\\ -\omega\left(1-2\nu\dfrac{\rho^2}{a^2}\right)\Big[\!\Big[\, n^2\,\mathring{a}_t^{\mp}\,\Big]\!\Big] \end{pmatrix}. \tag{3.36}$$

These expressions can be used in Equation (2.44) to compute the matrix $\mathcal{M}$ to obtain an explicit form of the propagation law given by Equation (2.43)–Equation (2.44); equivalently (2.45)-(2.46). Since the dispersion relation can only be solved numerically and the integrals arising here admit no concise explicit form, we evaluate $\mathcal{M}$ numerically. Concrete numerical results for a range of fiber parameters, including those relevant for the GRAVITES experiment[26], are presented in Section 3.3 and Figure 1.2–Figure 1.3.

3.2 Photoelasticity

We introduced the constitutive tensor for linear dielectric media in (2.2), specializing so far to isotropic media. Now, we consider small deviations from an ideal, isotropic, non-magnetic dielectric, writing the constitutive tensor as

$$\chi^{\mu\nu\rho\sigma} = \chi^{\mu\nu\rho\sigma}_{\text{isotropic}} + \varepsilon\delta\chi^{\mu\nu\rho\sigma}, \tag{3.37}$$

where ε is the same small expansion parameter introduced in (2.29), with a tensor field $\delta\chi^{\mu\nu\rho\sigma}$ arising from the change in permittivity introduced by elastic deformations. Taking a perturbative expansion for the field strength tensor $F_{\mu\nu}$ as well, we can write (2.2) as

$$G^{\mu\nu} = \gamma^{\mu\rho}\gamma^{\nu\sigma}(\mathring{F}_{\rho\sigma} + \varepsilon\tilde{F}_{\rho\sigma}) + \varepsilon\delta\chi^{\mu\nu\rho\sigma}\,\mathring{F}_{\rho\sigma}, \tag{3.38}$$

so that, using (2.6), the gauge-fixed Equation (2.8) becomes

$$\Box_\gamma A_\beta = -2\gamma_{\beta\nu}\nabla_\mu(\varepsilon\delta\chi^{\mu\nu\rho\sigma}\,\partial_\rho \mathring{A}_\sigma) + O(\varepsilon^2). \tag{3.39}$$

We assume that the medium remains non-magnetic and induces no magneto-electric coupling, so that $\delta\chi^{\mu\nu\rho\sigma}$ takes the form

$$\varepsilon\delta\chi^{0i0j} = \delta\epsilon^{ij}, \qquad \delta\chi^{ijkl} = 0, \qquad \delta\chi^{0ijk} = 0, \tag{3.40}$$

where $\delta\epsilon^{ij}$ is the elastically induced change in the permittivity tensor. In the linear regime, $\delta\epsilon^{ij}$ is related to the material strain u_{kl} via the photoelasticity tensor p_{ijkl} [27, Appendix D]:

$$\delta(\epsilon^{-1})_{ij} = p_{ijkl}u_{kl}. \tag{3.41}$$

The components p_{ijkl} generally need to be determined empirically, though in the case of an isotropic solid they simplify to 28

$$\mathbf{p} = \begin{pmatrix} p_{11} & p_{12} & p_{12} & 0 & 0 & 0 \\ p_{12} & p_{11} & p_{12} & 0 & 0 & 0 \\ p_{12} & p_{12} & p_{11} & 0 & 0 & 0 \\ 0 & 0 & 0 & \frac{1}{2}(p_{11}-p_{12}) & 0 & 0 \\ 0 & 0 & 0 & 0 & \frac{1}{2}(p_{11}-p_{12}) & 0 \\ 0 & 0 & 0 & 0 & 0 & \frac{1}{2}(p_{11}-p_{12}) \end{pmatrix}, \tag{3.42}$$

in Voigt notation, where $11 \to 1$, $22 \to 2$, $33 \to 3$, $23 \to 4$, $13 \to 5$, $12 \to 6$. Alternatively, employing tensor notation, we introduce material constants p and q through the formula

$$\begin{aligned} p_{ijkl} &= pg_{ij}g_{kl} + q(g_{ik}g_{jl} + g_{il}g_{jk}) \\ &\equiv p_{12}g_{ij}g_{kl} + \frac{1}{2}(p_{11}-p_{12})(g_{ik}g_{jl} + g_{il}g_{jk}), \end{aligned} \tag{3.43}$$

where g_{ij} are the components of the spatial metric (equal to the Kronecker δ_{ij} in Cartesian coordinates). For the case of fused silica glass, as used in optical fibers, the photoelasticity tensor is characterized by 26,29

$$p_{1111} \equiv p_{11} = 0.121, \quad p \equiv p_{1122} \equiv p_{12} = 0.271, \quad q \equiv p_{1212} \equiv p_{33} = -0.075. \tag{3.44}$$

Note that p_{1212} is measured independently, but in good agreement with the isotropy assumption made in (3.43). The induced source terms for the perturbative calculation as determined via (3.40) and the strain tensor (3.9) are given by

$$\varepsilon\sum_t^{(\pm,0)} = -n^2\frac{(u_{xx}+u_{yy})\big|_{r=0}}{r^2}\Big\{2(p+q+pr^2\beta^2)a_t^{\pm}+r\Big(\pm\mathrm{i}\sqrt{2}(p+q)\omega a_\flat^{\pm} \mp\mathrm{i}\sqrt{2}(p+q)\omega a_\sharp^{\pm}+2pr\beta\omega a_z^{\pm}-\mathrm{i}(p+q)r[\sqrt{2}\omega\partial_r(a_\flat^{\pm}+a_\sharp^{\pm})-2\mathrm{i}\partial_r^2 a_t^{\pm}]\Big)\Big\}, \tag{3.45a}$$

$$\varepsilon\sum_z^{(\pm,0)} = (u_{xx}+u_{yy})\big|_{r=0}\,2n^4\omega p\left(\beta a_t^{\pm}+\omega a_z^{\pm}\right), \tag{3.45b}$$

$$\varepsilon\sum_\sharp^{(\pm,0)} = \frac{(u_{xx}+u_{yy})\big|_{r=0}}{r}(p+q)n^4\omega\left(2r\omega a_\sharp^{\pm}\pm\mathrm{i}\sqrt{2}\left[a_t^{\pm}\mp r\partial_r a_t^{\pm}\right]\right), \tag{3.45c}$$

$$\varepsilon\sum_\flat^{(\pm,0)} = \frac{(u_{xx}+u_{yy})\big|_{r=0}}{r}(p+q)n^4\omega\left(2r\omega a_\flat^{\pm}\mp\mathrm{i}\sqrt{2}\left[a_t^{\pm}\pm r\partial_r a_t^{\pm}\right]\right), \tag{3.45d}$$

as well as

$$\begin{aligned}\varepsilon\sum_t^{(+,2)} = -n^2\frac{(u_{xx}-u_{yy})\big|_{r=0}}{4r^2a^2}\times\Big\{&4\left[qr^2(1-2\nu)+pr^2(-1+r^2\beta^2)(-1+2\nu)-2qa^2\right]a_t^-\\&-8r^3\left[2q\nu+p(-1+2\nu)\right]\partial_r a_t^- +\left[4pr^4(1-2\nu)+4qr^2(-2r^2\nu+a^2)\right]\partial_r^2 a_t^-\\&+4pr^4\beta(-1+2\nu)\omega a_z^- -2\mathrm{i}\sqrt{2}(p+q)r^3(-1+2\nu)\omega a_\sharp^-\\&-2\mathrm{i}\sqrt{2}(p+q)r^4(-1+2\nu)\omega\partial_r a_\sharp^- -\mathrm{i}\sqrt{2}\omega r\left[2r^2(p(-3+6\nu)+q(-1+6\nu))+4qa^2\right]a_\flat^-\\&-2\mathrm{i}\sqrt{2}r^2\omega\left[pr^2(-1+2\nu)+qr^2(1+2\nu)-2qa^2\right]\partial_r a_\flat^-\Big\},\end{aligned} \tag{3.46a}$$

$$\begin{aligned}\varepsilon\sum_t^{(-,2)} = -n^2\frac{(u_{xx}-u_{yy})\big|_{r=0}}{4r^2a^2}\times\Big\{&4\left[qr^2(1-2\nu)+pr^2(-1+r^2\beta^2)(-1+2\nu)-2qa^2\right]a_t^+\\&-8r^3\left[2q\nu+p(-1+2\nu)\right]\partial_r a_t^+ +\left[4pr^4(1-2\nu)+4qr^2(-2r^2\nu+a^2)\right]\partial_r^2 a_t^+\\&+4pr^4\beta(-1+2\nu)\omega a_z^+ -2\mathrm{i}\sqrt{2}(p+q)r^3(-1+2\nu)\omega a_\flat^+\\&-2\mathrm{i}\sqrt{2}(p+q)r^4(-1+2\nu)\omega\partial_r a_\flat^+ -\mathrm{i}\sqrt{2}\omega r\left[2r^2(p(-3+6\nu)+q(-1+6\nu))+4qa^2\right]a_\sharp^+\\&-2\mathrm{i}\sqrt{2}r^2\omega\left[pr^2(-1+2\nu)+qr^2(1+2\nu)-2qa^2\right]\partial_r a_\sharp^+\Big\},\end{aligned} \tag{3.46b}$$

$$\varepsilon\sum_z^{(\pm,2)} = -\frac{(u_{xx}-u_{yy})\big|_{r=0}}{a^2}p(1-2\nu)n^4\omega r^2\left(\beta\mathring{a}_t^{\mp}+\omega\mathring{a}_z^{\mp}\right), \tag{3.46c}$$

$$\varepsilon\sum_\sharp^{(+,2)} = -\frac{(u_{xx}-u_{yy})\big|_{r=0}}{2a^2}(1-2\nu)(q+p)n^4\omega r\left[2r\omega\mathring{a}_\sharp^- -\mathrm{i}\sqrt{2}\left(\mathring{a}_t^- +r\partial_r\mathring{a}_t^-\right)\right], \tag{3.46d}$$

$$\varepsilon\sum_\flat^{(-,2)} = -\frac{(u_{xx}-u_{yy})\big|_{r=0}}{2a^2}(1-2\nu)(q+p)n^4\omega r\left[2r\omega\mathring{a}_\flat^+ -\mathrm{i}\sqrt{2}\left(\mathring{a}_t^+ +r\partial_r\mathring{a}_t^+\right)\right], \tag{3.46e}$$

$$\begin{aligned}\varepsilon\sum_\flat^{(+,2)} = -\frac{(u_{xx}-u_{yy})\big|_{r=0}}{2ra^2}n^4\omega\times\Big[&2(q+p)r^3(1-2\nu)\omega\mathring{a}_\flat^- +4qr(a^2-r^2)\omega\mathring{a}_\sharp^-\\&-\mathrm{i}\sqrt{2}\left([2qa^2-(3q+p)r^2+2(q+p)r^2\nu]\mathring{a}_t^- +r[2qa^2-(q-p)r^2-2(q+p)r^2\nu]\partial_r\mathring{a}_t^-\right)\Big],\end{aligned} \tag{3.46f}$$

$$\varepsilon\sum_{\sharp}^{(-,2)} = -\frac{(u_{xx}-u_{yy})\big|_{r=0}}{2ra^2}n^4\omega\times\Bigg[2(q+p)r^3(1-2\nu)\omega\,\mathring{a}_{\sharp}^{+}+4qr(a^2-r^2)\omega\,\mathring{a}_{\flat}^{+}$$
$$-\mathrm{i}\sqrt{2}\Big([2qa^2-(3q+p)r^2+2(q+p)r^2\nu]\mathring{a}_t^{+}+r[2qa^2-(q-p)r^2-2(q+p)r^2\nu]\partial_r\mathring{a}_t^{+}\Big)\Bigg]. \quad (3.46g)$$

Further, for the correction terms arising for the interface conditions (2.39) we find explicitly

$$\tilde{\Gamma}^{(\pm,0)}[\mathring{a}^{\pm}] = 2(u_{xx}+u_{yy})\big|_{r=0}(p+q)\begin{pmatrix}0\\0\\0\\0\\\Big[\!\Big[n^4[\partial_r\mathring{a}_t^{\pm}+\frac{\mathrm{i}\omega}{\sqrt{2}}(\mathring{a}_{\sharp}^{\pm}+\mathring{a}_{\flat}^{\pm})]\Big]\!\Big]\\0\\0\\0\end{pmatrix}, \quad (3.47)$$

and

$$\tilde{\Gamma}_5^{(+,2)}[\mathring{a}^{-}] = -\frac{(u_{xx}-u_{yy})\big|_{r=0}}{\rho a^2}\Big[\!\Big[n^4\Big[q(r^2-a^2)\mathring{a}_t^{-}+r\Big(r^2(-p+2(p+q)\nu)-qa^2\Big)\partial_r\mathring{a}_t^{-}$$
$$+\frac{\mathrm{i}\omega}{\sqrt{2}}(p+q)r^3\big(-1+2\nu\big)\mathring{a}_{\flat}^{-}+\frac{\mathrm{i}\omega}{\sqrt{2}}r\Big(r^2\Big(-p+q+2\nu\big(p+q\big)\Big)-2qa^2\Big)\mathring{a}_{\sharp}^{-}\Big]\Big]\!\Big], \quad (3.48a)$$

$$\tilde{\Gamma}_5^{(-,2)}[\mathring{a}^{+}] = -\frac{(u_{xx}-u_{yy})\big|_{r=0}}{\rho a^2}\Big[\!\Big[n^4\Big[q(r^2-a^2)\mathring{a}_t^{+}+r\Big(r^2(-p+2(p+q)\nu)-qa^2\Big)\partial_r\mathring{a}_t^{+}$$
$$+\frac{\mathrm{i}\omega}{\sqrt{2}}(p+q)r^3\big(-1+2\nu\big)\mathring{a}_{\sharp}^{+}+\frac{\mathrm{i}\omega}{\sqrt{2}}r\Big(r^2\Big(-p+q+2\nu\big(p+q\big)\Big)-2qa^2\Big)\mathring{a}_{\flat}^{+}\Big]\Big]\!\Big], \quad (3.48b)$$

with the remaining components of $\tilde{\Gamma}^{(\pm,2)}$ vanishing identically.

Based on these source terms, Equation (2.44) determining the transport matrix for the Jones vector can be evaluated numerically by inserting the relevant Bessel functions and integrating. We find that the matrix $\mathcal{M}$ in (2.44) has the form

$$\mathcal{M} = \begin{pmatrix}\xi_p(u_{xx}+u_{yy})\big|_{r=0} & \xi_b(u_{xx}-u_{yy})\big|_{r=0}\\ \xi_b(u_{xx}-u_{yy})\big|_{r=0} & \xi_p(u_{xx}+u_{yy})\big|_{r=0}\end{pmatrix}. \quad (3.49)$$

The corresponding matrix $\hat{\mathcal{M}}$ entering the propagation law (2.45) in Cartesian coordinates thus takes the form

$$\hat{\mathcal{M}} = \xi_p(u_{xx}+u_{yy})\big|_{r=0}\begin{pmatrix}1&0\\0&1\end{pmatrix}+\xi_b(u_{xx}-u_{yy})\big|_{r=0}\begin{pmatrix}1&0\\0&-1\end{pmatrix}. \quad (3.50)$$

Here, ξ_p, ξ_b are coefficients that depend only on the fiber core radius, its unperturbed refractive indices, and the optical frequency of the fiber mode. Numerical results are presented in Section 3.3.

Since the unperturbed solutions described in Section 2.2 are confined to a small region around the fiber's axis, with the modes decaying exponentially in the cladding, it is natural to consider an approximate form of the above expressions that is valid for $r \ll a$. Using this *confinement approximation*, the strain components take the form

$$u_{rr} = \mu^{-1}\big[(1-2\nu)d_0 - \mu\nu\kappa + \mu(1+\nu)\alpha\delta\mathrm{T} + b_2\cos(2\theta)\big], \quad (3.51a)$$

$$u_{r\theta} = -\mu^{-1} b_2 \sin(2\theta)\,, \tag{3.51b}$$

$$u_{\theta\theta} = \mu^{-1}\left[(1-2\nu)d_0 - \mu\nu\kappa + \mu(1+\nu)\alpha\delta\mathrm{T} - b_2\cos(2\theta)\right]. \tag{3.51c}$$

Thus, the source terms for $\Delta m = 0$ are identical to (3.46) and (3.48), while $\sum_b^{(\pm,2)}$ and $\tilde{\Gamma}^{(\pm,2)}$ simplify significantly to

$$\varepsilon\sum_t^{(+,2)} = \frac{qn^2}{r^2}(u_{xx}-u_{yy})\Big|_{r=0}\left\{2a_t^- - r^2\partial_r^2 a_t^- + \mathrm{i}\sqrt{2}\omega r\left(a_\sharp^- - r\partial_r a_\sharp^-\right)\right\}, \tag{3.52a}$$

$$\varepsilon\sum_t^{(-,2)} = \frac{qn^2}{r^2}(u_{xx}-u_{yy})\Big|_{r=0}\left\{2a_t^+ - r^2\partial_r^2 a_t^+ + \mathrm{i}\sqrt{2}\omega r\left(a_\flat^+ - r\partial_r a_\flat^+\right)\right\}, \tag{3.52b}$$

$$\varepsilon\sum_z^{(\pm,2)} = 0, \tag{3.52c}$$

$$\varepsilon\sum_\sharp^{(+,2)} = 0, \tag{3.52d}$$

$$\varepsilon\sum_\flat^{(-,2)} = 0, \tag{3.52e}$$

$$\varepsilon\sum_\flat^{(+,2)} = -\frac{qn^4\omega}{r}(u_{xx}-u_{yy})\Big|_{r=0}\left[2r\omega a_\sharp^- - \mathrm{i}\sqrt{2}\left(a_t^- + r\partial_r a_t^-\right)\right], \tag{3.52f}$$

$$\varepsilon\sum_\sharp^{(-,2)} = -\frac{qn^4\omega}{r}(u_{xx}-u_{yy})\Big|_{r=0}\left[2r\omega a_\flat^+ - \mathrm{i}\sqrt{2}\left(a_t^+ + r\partial_r a_t^+\right)\right], \tag{3.52g}$$

and

$$\tilde{\Gamma}^{(\pm,2)}[\mathring{a}^{\mp}] = -\frac{q}{\rho}(u_{xx}-u_{yy})\Big|_{r=0}\begin{pmatrix} 0\\0\\0\\0\\ \left[\!\left[\, n^4[\mathring{a}_t^{\mp} + r\partial_r\,\mathring{a}_t^{\mp} + \mathrm{i}\sqrt{2}r\omega\,\mathring{a}_\flat^{\mp}]\,\right]\!\right]\\ 0\\0\\0 \end{pmatrix}, \tag{3.53}$$

The numerical results produced in Table 3.3 show good agreement between the confinement approximation and the full solution.

3.3 Numerical results

The Section 3.1 and Section 3.2 provide explicit expressions for the Σ- and $\tilde{\Gamma}$-terms that enter the matrix $\mathcal{M}$, defined in Equation (2.44), which determines the propagation law of light polarization according to Equation (2.43) and Equation (2.45). Here we present numerical values based on the material properties of silica oxide glass given in Table 3.1 and the experimental parameters of GRAVITES given in Table 3.2. The values for δg, δp and δT correspond to a height difference of 1m for an experiment without thermal insulation and pressure control. We expect the measurement arm to be raised, as opposed to lowered, from its calibrations height, leading to negativ signs for these quantities. Since the response of the system is linear in the environmental parameters, these numbers can directly be used to determine the constraints on the experimental setup so that environmental fluctuations do not overwhelm the signal of interest.

The numerical values determined in this work are juxtaposed in Table 3.3 with the results of Ref. 7, where the change of length of the optical fiber has been determined.

Table 3.2. Parameters for the GRAVITES experiment[4]. The last three lines correspond to a difference of height of 1 meter; the last two lines correspond to displacement in an unshielded ambient atmosphere at sea level.

Fiber outer radius a	62.5 μm
Fiber core radius ρ	4.1 μm
Core refractive index n_1	1.4712
Cladding refractive index n_2	1.4659
Fiber length L	10^5 m
Propagation constant β	6×10^6 m^{-1}
Wavelength λ	1.55 μm
Variation in grav. acceleration, δg	–3 μm s^{-2}
Variation in pressure, δp	–10 Pa
Variation in temperature, δT	-10^{-2} K

Table 3.3. Estimates for the phases, in radians, for an unshielded version of the GRAVITES experiment described in 4. The phase shifts arising from the longitudinal fiber expansion were computed in Ref. 7 The first column differs due to a correction of the linear thermal expansion coefficient α; the remaining shifts are determined in this work. Temperature and pressure differences over a vertical separation of 1m give rise to phase shifts via elastic deformations of the fiber and induced photoelastic effects; gravity gradients induce in-homogeneities and thus give rise to both phase perturbations and birefringence effects. Confinement approximation refers to (3.52) wherein the material strain components are expanded for $r \ll a$.

Gravitational phase shift	**-6.52×10^{-5}**			
Systematic effects	**Temperature**	**Pressure**	**Gravity gradient**	
	Phase	**Phase**	**Phase**	**Birefringence**
Longitudinal expansion[7]	–3240	–28	-7.0×10^{-7}	
Geometric deformation	–8.7	0.15	3.0×10^{-9}	-2.42×10^{-11}
Photoelasticity	–3190	53	1.1×10^{-6}	1.27×10^{-6}
Photoelasticity confinement approx.	–3190	53	1.1×10^{-6}	1.28×10^{-6}

In Figure 1.2 and Figure 1.3 we provide plots showing how a change in fiber parameters affects these values. Both for phase and birefringence the effect is essentially due to the photoelastic material response, as the contribution arising from the core-cladding interface deformation is smaller by four orders of magnitude. Additionally, this effect is practically independent of the fiber's material indices n_1 and n_2.

The phase information in Table 3.3 can alternatively be expressed in the form of the following equation,

$$\begin{aligned}\frac{\Delta\varphi}{L/\mathrm{km}} = &-[(3.24)_\ell + (8.7\times10^{-3})_g + (3.19)_p]\left(\frac{\Delta T}{K}\right)\\ &-[(2.8\times10^{-5})_\ell - (1.5\times10^{-7})_g - (5.3\times10^{-5})_p]\left(\frac{\Delta \mathfrak{p}}{Pa}\right)\\ &-[(2.29\times10^{-5})_\ell - (9.81\times10^{-8})_g - (3.6\times10^{-5})_p]\left(\frac{\Delta g}{g}\right)\end{aligned}$$

where the subscript ℓ refers to the contributions arising from longitudinal expansion, g to those from geometric deformation of the fiber cross-section, and p to photoelasticity.

Our calculations show that elastically induced birefringence is too small to be detectable in the currently planned experiments.

In an unshielded environment at sea level, with δT and δp corresponding to a vertical displacement by one meter in the atmosphere of the Earth, and with the material parameters as given in Table 3.2 the overall temperature-induced phase-shift is ~10^8 times the gravitational phase-shift of interest, while the overall pressure-induced phase shift is ~10^6 larger. Clearly no conclusions can be drawn from an experiment carried out in such an environment.

In any case, when taken at face value, the numbers in Table 3.3 constitute a serious challenge for a suitably shielded experiment, carried-out in a controlled environment, possibly in vacuum, where all the numbers will be scaled down. We further note that temperature variations can be mitigated by heating and may be diminished by undercutting the thermal equilibrium timescales involved. Moreover, we expect the phase shifts arising from the change of length to be overinflated for at least two reasons. First, the calculations allow for an unrestricted elongation of the fiber, which will not happen because of friction (we note that the latter seems difficult to model from first principles). Next, there is a question of time scales involved, as a change of the environment will not lead to an instantaneous change of length of the fiber.

We believe that our simple model here is useful in drawing attention to the need to mitigate the environmental effects in any precision experiments involving waveguides.

4 Conclusion

We solved Maxwell's equations with small source terms in an optical fiber background to first order in a perturbation scheme. We gave a general expression of the propagation of the Jones vector, which encodes changes in phase and birefringence, along the axis of the fiber to first order in perturbation theory – (2.45).

Using results derived in 7 for elastic deformations of cylinders we give formulas for the explicit source terms corresponding to interface deformations of the optical fiber and stress induces changes in the optical properties of the waveguide.

As a practical application of these findings we compute the expected changes in phase and birefringence due to elasticity effects for a range of fiber parameters in Figure 1.2–Figure 1.3 and concretely for the GRAVITES experiment[4] in Table 3.3. Concerning the effect of temperature changes we note that the results here are restricted to elastic contributions and do not encompass the full thermo-optic effect. Experimentally it is known that the longitudinal thermal expansion contributes about 5% to the total temperature dependence of the optical phase in fused silica fibers[8]. Our calculations show that the contribution of photoelasticity is on the same order; this differs from material to material[9].

Ethics and consent

Ethical approval and consent were not required.

Data availability

No data are associated with this article. This is purely mathematical/ theoretical work and as such there is no underlying data. All numerical results can be reproduced from the equations we derive.

References

1. Cromb M, Restuccia S, Gibson GM, *et al.*: **Mechanical rotation modifies the manifestation of photon entanglement.** *Phys Rev Res.* 2023; **5**(2): L022005.
Publisher Full Text
2. Fink M, Steinlechner F, Handsteiner J, *et al.*: **Entanglement-enhanced optical gyroscope.** *New J Phys.* 2019; **21**(5): 053010.
Publisher Full Text
3. Silvestri R, Yu H, Strömberg T, *et al.*: **Experimental observation of Earth's rotation with quantum entanglement.** *Sci Adv.* 2024; **10**(24): eado0215.
PubMed Abstract | **Publisher Full Text** | **Free Full Text**
4. Hilweg C, Massa F, Martynov D, *et al.*: **Gravitationally induced phase shift on a single photon.** *New J Phys.* 2017; **19**(3): 033028.
Publisher Full Text
5. Polini E, Macri D, Yin X, *et al.*: **Large-scale fiber interferometry to measure the gravitationally induced phase shift on entangled**

photons. In: *Quantum 2.0 Conference and Exhibition*. Optica Publishing Group, 2024; QTh4C.3.
Publisher Full Text

6. Hilweg C, Shadmany D, Walther P, *et al.*: **Limits and prospects for long-baseline optical fiber interferometry.** *Optica.* 2022; **9**(11): 1238–1252.
Publisher Full Text

7. Barzegar H, Chruściel PT, Steininger E: **On elastic deformations of cylindrical bodies under the influence of the gravitational field [version 1; peer review: 1 approved, 2 approved with reservations].** *Open Res Eur.* 2024; **4**: 98.
PubMed Abstract | **Publisher Full Text** | **Free Full Text**

8. Wang W, Yu Y, Geng Y, *et al.*: **Measurements of thermo-optic coefficient of standard single mode fiber in large temperature range.** In: *2015 international conference on optical instruments and technology: optical sensors and applications.* International Society for Optics and Photonics, SPIE, 2015; **9620**: 96200Y.
Publisher Full Text

9. Waxler RM, Cleek GW: **The effect of temperature and pressure on the refractive index of some oxide glasses.** *J Res Natl Bur Stand A Phys Chem.* 1973; **77A**(6): 755–763.
PubMed Abstract | **Publisher Full Text** | **Free Full Text**

10. Mieling TB: **Gupta-Bleuler quantization of the electromagnetic field in curved space-times with applications to gravitational photon interferometry**. Doctoral thesis, University of Vienna, 2023.
Publisher Full Text

11. Mieling TB, Hudelist M: **Fiber optics in curved space-times.** *Phys Rev Res.* 2025; **7**(1): 013162.
Publisher Full Text

12. Mieling TB, Oancea MA: **Polarization transport in optical fibers beyond Rytov's law.** *Phys Rev Res.* 2023; **5**(2): 023140.
Publisher Full Text

13. Post EJ: **Formal structure of electromagnetics**. North-Holland, 1962.
Reference Source

14. Senior JM, Jamro MY: **Optical fiber communications**. Pearson Education, 3 edition, 2009.
Reference Source

15. Li X, Huang X, Hu X, *et al.*: **Recent progress on mid-infrared pulsed fiber lasers and the applications.** *Opt Laser Technol.* 2023; **158**(Part B): 108898.
Publisher Full Text

16. Song Y, Wang Z, Wang C, *et al.*: **Recent progress on optical rogue waves in fiber lasers: status, challenges, and perspectives.** *Adv Photonics.* 2020; **2**(2): 024001.
Publisher Full Text

17. Gordon W: **Zur Lichtfortpflanzung nach der Relativitätstheorie.** *Ann Phys.* 1923; **377**(22): 421–456.
Publisher Full Text

18. Liu JM: **Photonic devices**. Cambridge University Press, 2005.
Reference Source

19. Mieling TB: **Gupta-Bleuler quantization of optical fibers in weak gravitational fields.** *Phys Rev A.* 2022; **106**(6): 063511.
Publisher Full Text

20. Bender CM, Orszag SA: **Advanced mathematical methods for scientists and engineers**. *International Series in Pure and Applied Mathematics*. McGraw-Hill, 1978.
Reference Source

21. Landau LD, Lifshitz EM: **Theory of elasticity, volume 7 of course of theoretical physics**. Elsevier Butterworth-Heinemann, 1986.
Reference Source

22. Sadd MH: **Elasticity: theory, applications and numerics**. Academic Press, second edition, 2009.
Publisher Full Text

23. Zhenye W, Shiping L: **The generalized plane strain problem and its application in three-dimensional stress measurement.** *International Journal of Rock Mechanics and Mining Sciences & Geomechanics Abstracts.* 1990; **27**(1): 43–49.
Publisher Full Text

24. Michell JH: **On the direct determination of stress in an elastic solid, with application to the theory of plates.** *P Lond Math Soc.* 1899; **s1-31**(1): 100–124.
Publisher Full Text

25. Crystran Ltd: **Silica glass (sio_2)**. Data Sheet, 2018.
Reference Source

26. Biegelsen DK: **Photoelastic tensor of silicon and the volume dependence of the average gap.** *Phys Rev Lett.* 1974; **32**: 1196–1199.
Publisher Full Text

27. Chen C: **Foundations for guided-wave optics.** Wiley, 2006.
Publisher Full Text

28. Narasimhamurty T: **Photoelastic and electro-optic properties of crystals**. Springer US, 1981.
Publisher Full Text

29. Primak W, Post D: **Photoelastic constants of vitreous silica and its elastic coefficient of refractive index.** *J Appl Phys.* 1959; **30**(5): 779–788.
Publisher Full Text

Open Peer Review

Current Peer Review Status: ✔ ✔ ✔

Version 2

Reviewer Report 10 September 2025

https://doi.org/10.21956/openreseurope.22625.r58210

© **2025 Maitra M.** This is an open access peer review report distributed under the terms of the Creative Commons Attribution License, which permits unrestricted use, distribution, and reproduction in any medium, provided the original work is properly cited.

✔ **Matthew Maitra**
ETH Zurich, Zürich, Zurich, Switzerland

I consider the revisions to be appropriate.

Competing Interests: No competing interests were disclosed.

Reviewer Expertise: Continuum mechanics; numerical methods for PDEs; some expertise in general relativity

I confirm that I have read this submission and believe that I have an appropriate level of expertise to confirm that it is of an acceptable scientific standard.

Reviewer Report 29 August 2025

https://doi.org/10.21956/openreseurope.22625.r58209

© **2025 Rajan M.** This is an open access peer review report distributed under the terms of the Creative Commons Attribution License, which permits unrestricted use, distribution, and reproduction in any medium, provided the original work is properly cited.

✔ **M. S. Mani Rajan**
Anna University, Ramanathapuram, India

1. Typo error in the Eqn (2.29)
2. In birefringence optical fibers, there is always more than one mode propagation is possible. This means that theoretical representation of multi mode propagation is can be described by coupled equation. But why authors didn't use coupled systems.
3. Importance of GRAVITES experiment should be discussed.

Competing Interests: No competing interests were disclosed.

Reviewer Expertise: Nonlinear Fiber Optics and Fiber sensor

I confirm that I have read this submission and believe that I have an appropriate level of expertise to confirm that it is of an acceptable scientific standard.

Version 1

Reviewer Report 25 June 2025

https://doi.org/10.21956/openreseurope.21009.r53942

© 2025 Maitra M. This is an open access peer review report distributed under the terms of the Creative Commons Attribution License, which permits unrestricted use, distribution, and reproduction in any medium, provided the original work is properly cited.

?

Matthew Maitra
ETH Zurich, Zürich, Zurich, Switzerland

SUMMARY

Steininger, Mieling and Chruściel derive the phase-shifts on photons passing through optical fibres subject to small elastic deformations. They do so via a multiple-scale perturbative scheme. They then use the results to discuss the associated systematic effects on the upcoming GRAVITES experiment.

DISCUSSION

The manuscript is well-written, providing good explanation of the methods employed. I have not gone through every line of algebra (!) but it is clear from the text that the authors are in command of the theory (note also that they have already published multiple methodological ingredients of the present manuscript). Section 2 in particular is exceptionally clearly written -- not an easy feat given how fiddly multiple-scale analysis can get. Section 3 also gives a good discussion of the derivation of the terms needed within Section 2's final expressions (with a couple of caveats discussed below). Similarly, Tables 3.2 and 3.3 give a good overview of the implications for GRAVITES, subject to some caveats.

1: Transformed interface terms (Section 3)

Section 3's discussion of elasticity is conceptually sound. But in general, Section 3.1.1 needs to draw the same crystal-clear distinction between physical and referential quantities that is drawn in the preceding subsubsection on ``The equations''. See the following.

1a

I find eq.(3.27) to be misleading. It would be much clearer to me if \chi, A and G all had overbars and different brackets were used. This would help to emphasise that these are the conditions at the *physical* core-cladding interface, as distinct from the reference interface r = \rho that the physical conditions are transformed onto.

For what it's worth, I would suggest that quantities associated with the zeroth-order reference have circle-diacritics while exact, physical quantities are simply unadorned. That would mesh well with Section 2.

1b

The wording around eq.(3.29) is a little awkward. \overline{A}_{\mu} is continuous across the *physical* interface, and since the cladding and core only differ in their optical properties (Table 3.2) there should be no discontinuity in the elastic deformation across the reference interface. From eq.(3.17) it then follows directly that A_{\mu} *is* continuous; this is not an assumption. (Unless the assumption is that the core and cladding have identical elastic properties; if so then please make explicit.)

1c (tangential remark on layout)

In section 3.1 we currently have ``The equations'' without a subsection heading, followed by ``Boundary conditions'' as Section 3.1.1. This seems excessively asymmetrical.

2: Implications for GRAVITES

2a

From the last sentence of the first paragraph of Section 3.3, ``the response of the system is linear in the environmental parameters, [so] these numbers can directly be used to determine the constraints on the experimental setup so that environmental fluctuations do not overwhelm the signal of interest.'' Now, if I interpret Table 3.3 correctly, then the overall temperature-induced phase-shift is O(10^{8}) times the gravitational phase-shift of interest, while the overall pressure-induced phase shift is O(10^{6}) larger, with \delta T and \delta p as given in Table 3.2. For the systematic errors related to temperature and pressure each to be \approx 10% of the interesting signal, it would therefore seem that GRAVITES would need \delta T \approx 10^{-11}K and \delta P \approx 10^{-6}Pa.

Is this feasible? Not being an experimentalist I have no feel for this. If there is one message that this paper should communicate to any reader, it is surely the implication for GRAVITES of the paper's hard analysis. Therefore I would very much like to see a discussion along the lines of the previous paragraph. It is too important not to state explicitly.

2b (tangential comment)

When I reviewed the previous paper in this series (ref. [6]) I had some misgivings about approximating the fibre as straight, but now that I see how tiny a relative effect the ``Geometric deformation'' has on the phase shift, those misgivings are basically gone.

CONCLUSION

I would be glad to see this interesting work indexed subject to adequate treatment of the points mentioned above.

Is the work clearly and accurately presented and does it cite the current literature?
Partly

Is the study design appropriate and does the work have academic merit?
Yes

Are sufficient details of methods and analysis provided to allow replication by others?
Yes

If applicable, is the statistical analysis and its interpretation appropriate?
Not applicable

Are all the source data underlying the results available to ensure full reproducibility?
No source data required

Are the conclusions drawn adequately supported by the results?
Yes

Competing Interests: No competing interests were disclosed.

Reviewer Expertise: Continuum mechanics; numerical methods for PDEs; some expertise in general relativity

I confirm that I have read this submission and believe that I have an appropriate level of expertise to confirm that it is of an acceptable scientific standard, however I have significant reservations, as outlined above.

Reviewer Report 02 June 2025

https://doi.org/10.21956/openreseurope.21009.r53941

© 2025 Li X. This is an open access peer review report distributed under the terms of the Creative Commons Attribution License, which permits unrestricted use, distribution, and reproduction in any medium, provided the original work is properly cited.

Xiaohui Li
Shaanxi Normal University, Xi'an, Shaanxi, China

This paper investigates the phase shifts and birefringence phenomena in optical fibers under elastic deformation (e.g., due to temperature, pressure, and gravity variations). Through theoretical analysis and numerical calculations, the authors derive the light propagation

characteristics of fibers under elastic deformation and provide specific constraints for environmental control in fiber interferometers. The results demonstrate that temperature and pressure changes primarily affect the optical performance of fibers through elastic deformation and the photoelastic effect, while gravity gradients induce phase shifts and birefringence. These findings are significant for improving the precision and reliability of fiber interferometers, particularly in long-baseline fiber interferometry and gravitational experiments. Below are some suggestions for the paper:

1. The authors are advised to compare their work with recent related studies, such as *Adv. Opt. Mater.* **10**(24), 2201812 (2022); *Optics & Laser Technology*, **151**, 108016 (2022); *Optics & Laser Technology*, **158**, Part B, 108898 (2023); *Ultrafast Science*, **2022**, 9767251, 16 (2022); *Ultrafast Science*, **2022**, 9870325, 6 (2022); *Advanced Photonics*, **2**(2), 024001 (2020); *Advanced Photonics* , **2**(1), 015001 (2020). Such comparisons would help readers better understand the innovations and contributions of this work.
2. The paper assumes the fiber is an ideal linear isotropic medium, which simplifies the problem to some extent. However, real fibers may exhibit nonlinear effects and anisotropy. It is recommended to discuss the limitations of these assumptions and explore how nonlinearity and anisotropy might influence the results. Future work could incorporate these effects to provide a more comprehensive description of the fiber's physical properties.
3. The paper mentions that temperature-induced phase shifts in fibers are primarily manifested through elastic deformation but does not fully address the thermo-optic effect. It is suggested that the discussion be expanded to include the direct impact of temperature changes on the fiber's refractive index, thereby providing a more complete assessment of temperature effects on fiber interferometers. References [24] and [25] could be cited to further analyze the contribution of temperature variations to refractive index changes and compare them with elastic effects.
4. The paper presents abundant numerical results, but their physical significance could be further analyzed. For instance, the impact of phase shifts and birefringence under different environmental variations on the measurement accuracy of fiber interferometers could be discussed in greater detail, along with potential experimental methods to compensate for or correct these effects. Additional figures or graphs illustrating the trends of phase shifts and birefringence under varying environmental parameters could enhance readers' intuitive understanding of the results.
5. The introduction provides an overview of the research background and motivation, but this section could be strengthened. A more detailed explanation of why studying phase shifts and birefringence in fibers under elastic deformation is crucial for fiber interferometer applications—particularly in quantum optics and gravitational experiments—would be beneficial. Citing more experimental studies to demonstrate the practical implications of these elastic effects could further contextualize the research and reinforce its significance.

References

1. Steininger E, Mieling T, Chruściel P: Elastically induced phase-shift and birefringence in optical fibers. *Open Research Europe*. 2025; **5**. Publisher Full Text

Is the work clearly and accurately presented and does it cite the current literature?

Yes

Is the study design appropriate and does the work have academic merit?

Yes

Are sufficient details of methods and analysis provided to allow replication by others?
Yes

If applicable, is the statistical analysis and its interpretation appropriate?
Yes

Are all the source data underlying the results available to ensure full reproducibility?
Partly

Are the conclusions drawn adequately supported by the results?
Yes

Competing Interests: No competing interests were disclosed.

Reviewer Expertise: This paper investigates the phase shifts and birefringence phenomena in optical fibers under elastic deformation (e.g., due to temperature, pressure, and gravity variations). Through theoretical analysis and numerical calculations, the authors derive the light propagation characteristics of fibers under elastic deformation and provide specific constraints for environmental control in fiber interferometers. The results demonstrate that temperature and pressure changes primarily affect the optical performance of fibers through elastic deformation and the photoelastic effect, while gravity gradients induce phase shifts and birefringence. These findings are significant for improving the precision and reliability of fiber interferometers, particularly in long-baseline fiber interferometry and gravitational experiments. Below are some suggestions for the paper:1. The authors are advised to compare their work with recent related studies, such as Adv. Opt. Mater. 10(24), 2201812 (2022); Optics & Laser Technology, 151, 108016 (2022); Optics & Laser Technology, 158, Part B, 108898 (2023); Ultrafast Science, 2022, 9767251, 16 (2022); Ultrafast Science, 2022, 9870325, 6 (2022); Advanced Photonics, 2(2), 024001 (2020); Advanced Photonics, 2(1), 015001 (2020). Such comparisons would help readers better understand the innovations and contributions of this work.2. The paper assumes the fiber is an ideal linear isotropic medium, which simplifies the problem to some extent. However, real fibers may exhibit nonlinear effects and anisotropy. It is recommended to discuss the limitations of these assumptions and explore how nonlinearity and anisotropy might influence the results. Future work could incorporate these effects to provide a more comprehensive description of the fiber's physical properties.3. The paper mentions that temperature-induced phase shifts in fibers are primarily manifested through elastic deformation but does not fully address the thermo-optic effect. It is suggested that the discussion be expanded to include the direct impact of temperature changes on the fiber's refractive index, thereby providing a more complete assessment of temperature effects on fiber interferometers. References [24] and [25] could be cited to further analyze the contribution of temperature variations to refractive index changes and compare them with elastic effects.4. The paper presents abundant numerical results, but their physical significance could be further analyzed. For instance, the impact of phase shifts and

birefringence under different environmental variations on the measurement accuracy of fiber interferometers could be discussed in greater detail, along with potential experimental methods to compensate for or correct these effects. Additional figures or graphs illustrating the trends of phase shifts and birefringence under varying environmental parameters could enhance readers' intuitive understanding of the results.5. The introduction provides an overview of the research background and motivation, but this section could be strengthened. A more detailed explanation of why studying phase shifts and birefringence in fibers under elastic deformation is crucial for fiber interferometer applications—particularly in quantum optics and gravitational experiments—would be beneficial. Citing more experimental studies to demonstrate the practical implications of these elastic effects could further contextualize the research and reinforce its significance.

I confirm that I have read this submission and believe that I have an appropriate level of expertise to confirm that it is of an acceptable scientific standard.

Reviewer Report 23 April 2025

https://doi.org/10.21956/openreseurope.21009.r53003

© 2025 Rajan M. This is an open access peer review report distributed under the terms of the Creative Commons Attribution License, which permits unrestricted use, distribution, and reproduction in any medium, provided the original work is properly cited.

?

M. S. Mani Rajan
Anna University, Ramanathapuram, India

Authors should reply to the following questions and improve the manuscript
1. Why authors consider the ideal optical fibers?
2. Typo error in many places. Example in Eqn. (2.29). Kindly check all equations.
3. Motivation of problem is not stated properly.
4. Why authors consider the linear media?. Optical fiber is a nonlinear medium. Justify.
5. Why authors describe dispersion less medium?.

Is the work clearly and accurately presented and does it cite the current literature?
Partly

Is the study design appropriate and does the work have academic merit?
Yes

Are sufficient details of methods and analysis provided to allow replication by others?
Partly

If applicable, is the statistical analysis and its interpretation appropriate?
Not applicable

Are all the source data underlying the results available to ensure full reproducibility?
No source data required

Are the conclusions drawn adequately supported by the results?
Partly

Competing Interests: No competing interests were disclosed.

Reviewer Expertise: Nonlinear Fiber Optics and Fiber sensor

I confirm that I have read this submission and believe that I have an appropriate level of expertise to confirm that it is of an acceptable scientific standard, however I have significant reservations, as outlined above.